LARS CONTRACT REPORT 060185

~~Not for Distribution~~
On NASA Technical Report Server

~~Anuta~~

LANDSAT-4/5 IMAGE DATA QUALITY ANALYSIS

TYPE III FINAL REPORT

NASA CONTRACT NAS5-26859

AUGUST 9, 1982 - DECEMBER 8, 1984

TO: NATIONAL AERONAUTICS & SPACE ADMINISTRATION
GODDARD SPACE FLIGHT CENTER
GREENBELT, MD 20771

BY: P.E. ANUTA AND STAFF
PURDUE UNIVERSITY
LABORATORY FOR APPLICATIONS OF REMOTE SENSING
1291 CUMBERLAND AVE.
WEST LAFAYETTE, IN 47906-1399

LARC CONTRACT REPORT 060185

SQ1

ERTS

E85-10105

NASA-CR-176264

LANDSAT-4/5 IMAGE DATA QUALITY ANALYSIS

TYPE III FINAL REPORT

NASA CONTRACT NAS5-26859

AUGUST 9, 1982 - DECEMBER 8, 1984

TO: NATIONAL AERONAUTICS & SPACE ADMINISTRATION

GODDARD SPACE FLIGHT CENTER

GREENBELT, MD 20771

BY: P.E. ANUTA AND STAFF

PURDUE UNIVERSITY

LABORATORY FOR APPLICATIONS OF REMOTE SENSING

1291 CUMBERLAND AVE.

WEST LAFAYETTE, IN 47906-1399

Star Information Form

1. Report No	2 Government Accession No	3. Recipient's Catalog No

4. Title and Subtitle	5. Report Date
Final Report for Landsat-4/5 Image Data Quality Analysis	12-8-84
	6. Performing Organization Code

7. Author(s)	8. Performing Organization Report No
P.E. Anuta and Staff	060185

9. Performing Organization Name and Address	10. Work Unit No
Laboratory for Applications of Remote Sensing Purdue University 1291 Cumberland Ave. West Lafayette, IN 47906-1399	11. Contract or Grant No NAS5-26859

12. Sponsoring Agency Name and Address	13. Type of Report and Period Covered
National Aeronautics and Space Administration Goddard Space Flight Center Greenbelt, MD 20771	Type III Final Report Contract 8-9-82/12-8-84
	14. Sponsoring Agency Code

15. Supplementary Notes

Original photography may be purchased
from EROS Data Center
Sioux Falls, SD 57198

16. Abstract

A Landsat Thematic Mapper quality evaluation study was conducted to determine the existence of geometric and radiometric sensor errors in data in the post-launch environment. The study began with the launch of Landsat-4. Several error conditions were found, including band-to-band misregistration and detector-to-detector radiometric calibration errors. These results were reported and used by NASA to update the system.

Similar analysis was made for the Landsat-5 Thematic Mapper and compared with results for Landsat-4. Remaining band-to-band misregistration was found to be within tolerances and detector-to-detector calibration errors were not severe but still existent. More coherent noise signals were observed in TM-5 than in TM-4, although the amplitude was generally less. The scan-direction differences observed in TM-4 were still evident in TM-5. The largest effect was in Band 4 where nearly a one digital count difference was observed.

Resolution estimation was carried out using roads in TM-5 for the primary focal plane bands rather than field edges as in TM-4. Estimates using roads gave better resolution than the ones using edges. Thermal IR band calibration studies were conducted and new nonlinear calibration procedures were defined for TM-5. The overall conclusion is that there are no first-order errors in TM-5 and any remaining problems are second or third order.

17. Key Words (Suggested by Author(s))	18. Distribution Statement
Thematic Mapper, band-to-band misregistration, detector-to-detector calibration, resolution estimation	

19. Security Classif. (of this report)	20. Security Classif. (of this page)	21. No. of Pages	22 Price
Unclassified	Unclassified		

*For sale by the National Technical Information Service, Springfield, Virginia 22161

NASA - JSC

NAS5-26859
LARS 060185

LANDSAT-4/5 IMAGE DATA QUALITY ANALYSIS

Type III Final Report

NASA Contract NAS5-26859

August 9, 1982 - December 8, 1984

To

NATIONAL AERONAUTICS AND SPACE ADMINISTRATION

GODDARD SPACE FLIGHT CENTER

Greenbelt, MD 20771

From

P.E. Anuta and Staff

PURDUE UNIVERSITY
Laboratory for Applications of Remote Sensing

1291 Cumberland Ave.
West Lafayette, IN 47906-1399

December 1984

LARS Contract Report 060185

LANDSAT-4/5 THEMATIC MAPPER DATA QUALITY ANALYSIS

Erick Malaret, Luis A. Bartolucci, D. Fabian Lozano
Paul E. Anuta, Clare D. McGillem

Laboratory for Applications of Remote Sensing
and
School of Electrical Engineering
Purdue University
West Lafayette, IN 47906-1399

ABSTRACT

A Landsat Thematic Mapper quality evaluation study was conducted to determine the existence of geometric and radiometric sensor errors in data in the post-launch environment. (The Landsat-4 Thematic Mapper will be denoted TM-4 and similarly for Landsat-5.) The study began with the launch of Landsat-4; several error conditions were found, including band-to-band geometric misregistration and detector-to-detector radiometric calibration errors. These results were reported (Anuta, 1984) and other investigators and used by NASA to update the system.

This paper describes similar analysis for the Landsat-5 Thematic Mapper and comparisons are made with results for Landsat-4. Remaining band-to-band misregistration was found to be within tolerances and detector-to-detector calibration errors were not severe but still existent. More coherent noise signals were observed in TM-5 than in TM-4, although the amplitude was generally less. The scan-direction differ-

ences observed in TM-4 were still evident in TM-5, the largest effect being in Band 4 where nearly a one digital count difference was observed. Resolution estimation was carried out using roads in TM-5 for the primary focal plane bands rather than field edges as in TM-4. Estimates using roads gave better resolution than the ones using edges. Thermal IR band calibration studies were conducted and new nonlinear calibration procedures were defined for TM-5. The overall conclusion is that there are no first-order errors in TM-5 and any remaining problems are second or third order.

Introduction

This paper describes analysis of Landsat 5 Thematic Mapper data to evaluate geometric and radiometric quality. In a previous paper (Anuta, 1984),* Landsat 4 Thematic Mapper and multispectral scanner data were analyzed for the geometric and radiometric quality and information content. The results of the Landsat 5 work are compared to that for the Landsat 4, so some of the material in the previous paper is repeated here. Not all the topics studied in the Landsat 4 study were repeated, so only a subset of the results are comparable. As a guide to the results in the two papers, the subjects are listed below, with those reported in this paper indicated in the second column.

* See Appendix for Landsat-4 results.

	IEEE GRS May 84	ASP Sept. 85
1. Effects of resampling (comparison of A & P tapes).....	X	
2. Band-to-band registration.....	X	X
3. Detector-to-detector calibration.....	X	X
4. Coherent-noise analysis.....	X	X
5. Spatial resolution estimation.....	X	X
6. Scan-angle effects.....	X	
7. Scan-direction effects.....	X	X
8. Spectral dimensionality.....	X	
9. Spectral separability.....	X	
10. Thermal calibration.....	X	X

The results of the Landsat-4 study revealed several geometric and radiometric errors which, when reported to NASA by the authors as well as by several other investigators, resulted in corrections and modifications that were incorporated in Landsat 4 ground processing and the Landsat 5 sensors. This study is a final evaluation of the success of these changes and the results indicate no significant problems with the TM system. Some second-order problems with noise and calibration exist and these are discussed.

Band-to-Band Misregistration

The importance of band-to-band registration is that it specifies the spatial alignment of all spectral bands in the system. Exact requirements for band-to-band misregistration were as follows[3]: "A point imaged in any of the first four spectral bands shall be registered to the same point in any of the other first four spectral bands within .2 IFOV along-track and across-track. This registration error includes the effects of all synchronizing and correcting signals developed by the instrument that are required to process the data into an image. Similarly Bands 5 and 7 shall be registered to Band 6 within .2 of Band 6 IFOV, and Band 5 shall be registered to the first four bands within .3 IFOV. These requirements shall be satisfied at least 90% of the time and apply to all points along a scan line." Visual blink comparison of the different bands in both TM-4 and TM-5 for registration accuracy was extremely good; detailed analysis was required to find subtle errors.

Band-to-band misregistration was assessed using a correlation algorithm capable of estimating shifts to subpixel accuracy and which can be applied row-wise or column-wise. The algorithm finds the lag at which the correlation coefficient between any two bands is maximum by using cubic spline interpolation. It was found that better results are obtained if the registration algorithm is applied to images in which discontinuities are enhanced by some kind of gradient operation technique. The gradient operation used was implemented as follows; if gi cor-

respond to the image plane of Band i, then for across-track measurements of misregistration, every row in g_i was convolved with

$$[\ -1\ \ 1\ \ 0\ ]$$

and the magnitude of the resulting image was taken. This is equivalent to computing the magnitude of the gradient along the rows of g_i. The advantage of this is that it enhances all the boundaries and sharp discontinuities in the image, which is exactly the kind of scene features an observer uses when evaluating misregistration by visual inspection. The gradient operator was applied row-wise for estimating the registration in the across-track direction or column-wise for the along-track direction.

The means and standard deviations of the shifts for blocks of 64x256 was computed using P-tape data from Illinois for both TM-4 and TM-5. Misregistration for the TM-4 have been previously assessed[4], and the possible existence of misregistration problems between the primary focal plane Bands (Bands 1-4) and Bands 5,7 was reported. More recent results obtained for TM-4 by preprocessing the data with a gradient operator indicate that Bands 1 through 4 are registered within the tolerance limits with Bands 5 and 7. Bands pairs 4,1 and 4,3 gave misregistration of at most .38 pixel, which is above the tolerance limit of .2 IFOV. This misregistration could result from the observed poor correlation between Bands 1,3 with Band 4 and therefore is not necessarily conclusive.

For TM-5 we found that the first four bands, which lie in the primary focal plane, have a mean misregistration of, at most, .07 pixel, which is well within the .2 pixel specification. Results for the estimated across- and along- track registration for TM-5 are presented in Table 1 and Table 2, where X_{ij} is the mean misregistration between Bands i and j, and $\sigma_{X_{ij}}$ is the corresponding standard deviation. Overall, the TM-5 complies very well with all the registration requirements for both along- and across-track directions.

Striping Effects

There are two basic types of striping effects that have been observed on TM-4 and TM-5 imagery. These are detector-to-detector striping and scan-to-scan striping (also called banding). The first is due to gain differences between the detectors in any given band, and the second to alternating levels of brightness related to the forward and reverse scanning operations.

TM-5 detector-to-detector striping and banding was assessed by computing the mean values for 256 consecutive scan lines over a Lake Michigan scene (July 18, 1984). This area was selected because of the low intensity level and small variation present on the signal, facilitating the study of banding and striping phenomena. Figures 1 and 2 show results obtained for TM-5 Bands 4 and 7. In Bands 4 and 7, the banding phenomenon was clearly seen, with an average difference between scans of

approximately .9 and .51 binary number. In Band 4 the difference was almost one binary number, which made it easily noticeable by visual inspection. Striping was also noticeable in these two bands. Band 5 showed striping formed mainly by a single detector, with a standard deviation of approximately .8 binary number. Also Bands 6 and 7 showed evidence of striping. In Band 2 an oscillation with a period of approximately 256 scan lines was observed. The differences in binary number observed in the TM-5 due to banding and striping are all below 1, indicating that relative calibration is very good.

For TM-4, banding and striping effects were also studied over the same area of Lake Michigan. In TM-4 banding was observed only on Band 4, while striping was present in all other bands. The striping observed in Bands 7,5,?,1 was due mainly to a single detector. With the exception of Band 7, the banding and striping deviation is below the one binary number range. For Band 7 striping due to a single detector was in some cases as big as 1.1 binary number.

Coherent Noise Analysis

Presence of coherent noise in the TM-4 has been reported by different researchers[4,5]. The source of this noise is believed to be related to specific electronic or mechanical oscillations in the system. TM-5 data were searched for the presence of coherent noise sources. An average power spectrum was estimated over a block of 256x256 in Lake Michigan. The power spectrum measurement used is given by

$$20\log_{10}\left[\frac{1}{N}\sum_{i=1}^{256} DFT(w_j g_{ij})\right] \quad 1 \le j \le 256$$

where g_{ij} is the image with corresponding row and column index i,j and w_{ij} is a Hamming window function. Figure 3 shows the estimated power spectrum for TM Band 3, where the presence of three noise frequencies can be easily seen with corresponding periods of 12.8, 6.24, and 5.12 pixel. The power in the TM-5 noise frequencies is nominally 5 to 7 db above the background noise level in Bands 2,3,4,5,7.

Table 3 compiles the different noise periods measured over Lake Michigan in both the TM-5 and TM-4. The measured noise periods in the TM-4 and TM-5 are not the same. The observed periods were too low to be attributed to jitter. No in-depth attempt was made here to find the source of this noise. Results are presented as evidence to aid researchers and data processing agencies in correcting for these anomalies.

Resolution Estimation in TM Data

One geometric parameter of particular interest is the actual in-flight resolution of the sensor system which includes all environmental and data processing factors. The resolution is determined by the point-spread function (PSF) of the system. This can be estimated in image data by observing the measured response to scene elements of known shape.

For a space-invariant PSF, the measured image in the spatial domain can be expressed as a convolution of the scene with the PSF, i.e.,

$$g(x,y) = h(x,y) * f(x,y)$$

where $f(x,y)$ is the earth scene, $h(x,y)$ is the overall PSF of the sensor system, and $g(x,y)$ is the resulting image.

Three scene elements that are useful for this type of analysis are:

1. An impulse represented by a narrow-width discontinuity along a row or column of the data, e.g., narrow roads.

2. A step function represented by an abrupt change in gray level along a row or column of the data.

3. A rectangular pulse represented by a sequence of two steps in opposite directions along a row or column of the data.

For our purposes, we estimated the line-spread function (LSF) in the direction normal to the discontinuity generated by any of the three suggested scene elements. If the LSF is known for many different orientation angles[2], then the two-dimensional PSF can be reconstructed.

It was observed by experimentation with the three types of scene elements that the step edge was the most desirable to use in Bands 5 and 7. In particular, agricultural field edges with high contrast fields of uniform texture were used. For Bands 1 through 4 the first type of scene element was used. To determine the LSF, subpixel sampling is

required since the sample rate of the TM is nominally the width of the predicted LSF. A procedure was defined to allow subpixel sampling of edges or roads (IEEE 1984). One critical aspect of the data extraction procedure is the accurate estimation of the scene element orientation, since any error here will propagate to the LSF estimate. Performance curves which relate the variance of the scene element orientation to the signal-to-noise ratio were obtained, and a discriminant function for scene element selection was developed[1]. The subpixel scheme was applied to scene elements in the Iowa and Illinois data sets. A set of dense samples was obtained for several scene elements in all bands, except Band 6. For the case of field edges, the LSF was estimated in earlier work[6,7] using a finite sum of basis functions or by relating the derivative of the system response to the LSF.

When a narrow road is used for estimating the LSF, it can be modeled as a narrow-width discontinuity superimposed on a constant background, i.e.,

$$f(x) = A\,\mathrm{rect}\left(\frac{x}{\tau}\right) + B$$

where τ is the width of the road, A is the amplitude of the discontinuity, and B is the constant background. The resolution of the TM is approximately 30 meters; therefore, if rural area roads with a width of approximately 6 to 7 meters are used, the system response can be used to establish upper bounds in the system resolution. The equivalent width of the LSF has been previously used to characterize the resolution of

the TM. It is interesting to see how the equivalent width of the TM to a narrow road can be related to the equivalent width of the actual LSF. It can be shown[1] that the exact relation is

$$W_{eq}(h) = \alpha W_{eq}(g) = \frac{1}{\tau}\int_{-\frac{\tau}{2}}^{\frac{\tau}{2}} \frac{h(\lambda)}{h(0)} d\lambda W_{eq}(g)$$

where α is going to be less or equal than one due to the monotonically decreasing behavior of the LSF as you move away from the origin. Since we do not know h offhand, α is not known exactly. But, for the case of τ = 6 meters and h given by a Gaussian function with half amplitude width of 1, we obtain = .995. This convinced us that narrow roads can be used for estimating the system resolution capabilities as long as the half-amplitude width of h is approximately equal to one or greater than one. The estimated LSF is given by a smoothed representation of the system response to the road.

Scene elements for the two cases considered were extracted from the Iowa and Illinois scenes. Figures 4 and 5 show the raw data for Bands 3 and 7. The resulting LSF, when cubic splines are used for smoothing, are shown in Figures 6 and 7. Table 4 is a compilation of the LSF half-amplitude widths estimates, using two types of smoothing algorithm, in the TM-5. The units used in this table are sampling intervals (si), where one si = 28.5 meter. As we concluded in earlier work for the TM-4, TM-5 resolution estimates also indicate that the actual overall

resolution is slightly less than the joint electronic and optical system resolution of 1 IFOV. This would be due to atmospheric and data processing effects or to the characteristics of the scene elements used.

Calibration of Landsat-5 TM Thermal IR Data

The procedures for calibration of the Landsat-4 TM thermal IR data and the resulting water temperature maps have been reported in a previous paper[4]. This paper deals with the calibration of the thermal IR data collected by the Thematic Mapper sensor on board Landsat-5 and it includes a description of the procedures developed for calibration, the results of calibrated thermal IR data, and a comparison of these procedures and results with those obtained from the Landsat TM-4 data.

Calibration Procedure

The calibration of the TM-4 thermal IR data was straight forward because the temperatures of the internal calibration sources (blackbodies) were known with reliability, i.e., 260 K and 320 K, which corres pond to the 0 and 255 digital count levels, respectively. On the other hand, the temperatures of the reference blackbodies for the TM-5 sensor were not known with a high degree of accuracy[8]. Therefore the first step in the calibration procedure involved the determination of these two reference tempertures for the TM-5 sensor.

To determine these temperatures, the minimum (Rmin.) and maximum (Rmax.) spectral radiances stored as radiometric calibration ancillary records on the P-tape CCTs[9] were used in conjunction with the results of the integration of Planck's equation for a bandwidth defined by the mean system response function of all four band-6 detectors. Table 5 shows the values (in mWatts/cm^2.sr. m) of the minimum and maximum spectral radiances corresponding to the 0 and 255 digital count levels for the TM-5 thermal IR band.

Table 5. Spectral Rmin. and Rmax. for the TM-5 Thermal IR Band

Rmin.(Spectral) =	0.1237800 mWatts/cm^2.sr.um
Rmax.(Spectral) =	1.5599560 mWatts/cm^2.sr.um

These spectral radiances were then converted to "in-band" radiances for a band defined by the mean system response function of all four detectors. The system response curves for the four detectors of both the Landsat 4 (protoflight) and Landsat-5 (flight) sensors are illustrated in Figure 8, and the "in-band" Rmin. and Rmax. radiances are given in Table 6.

Table 6. "In-Band" Rmin. and Rmax. for the TM-5 Thermal IR Band

Rmin.(In-Band) = 0.2438466 (mWatts/cm^2.sr.)	
Rmax.(In-Band) = 3.0731133 (mWatts/cm^2.sr.)	

These Rmin.(in-band) and Rmax.(in-band) radiances correspond to the amount of energy emitted by a blackbody radiating at 203.2 K and 341.2 K respectively, which should be the temperatures of the two internal calibration sources for the thermal IR band of the Landsat-5 Thematic Mapper sensor system, and they should correspond to the 0 and 255 digital count levels of the data.

Since the Thematic Mapper Product (P-tape) data have been radiometrically corrected so that there is a linear relationship between radiance and the corresponding digital counts (DC), the following linear transformation was derived for the conversion of digital counts into in-band radiances and vice versa:

$$R\ (\text{In-Band}) = (DC + 21.977) / 90.127 \qquad \text{Eq. 1}$$

Where, R = In-Band Radiance in mWatts/cm^2.sr.

DC = Digital Counts between 0 and 255

Planck's equation was integrated between 10.00 μm and 13.00 μm at spectral intervals of 0.01 μm and for a range of temperatures between 203.2 K and 341.2 K. The resulting "in-band radiances" were then multiplied by the system response values (the mean for all four TM-5 detectors) given by Markham and Barker[10], and then summed over the entire 10.00 μm and 13.00 μm temperature range, as illustrated by Equation 2.

$$W_{\overline{SR}} = \Sigma_i \left[\left(\int_{\lambda_L + i\Delta\lambda}^{\lambda_L + (i+1)\Delta\lambda} 2\pi c^2 \lambda^{-5} (e^{hc/\lambda kT} - 1)^{-1} \, d\lambda \right) \overline{SR}_i \right] \qquad \text{Eq. 2}$$

Where, W = In-band radiance in mWatts/cm^2.sr.

c = Speed of light

h = Planck's constant

λ = Wavelength

k = Boltzmann's constant

T = Temperature in degrees Kelvin

SR = System response (Markham and Barker[10])

λ_L = 10 m

$\Delta\lambda$ = .01 m

i = 1-300

The "in-band" radiances derived from Equation 2 can be closely approximated by "in-band" radiances produced by a square band with lower and upper limits located at the 50% cutoff of the system response curve, i.e., 10.42 μm and 12.45 μm, respectively.

As reported by Bartolucci et al.[11], the relationship between radiance (or digital counts) and temperature, for ranges of temperatures greater than 10 degrees Kelvin is not linear; therefore a quadratic and a cubic fit were derived to convert the TM-5 thermal IR band digital counts into radiant temperatures. Figure 9 shows both the quadratic and cubic regression curves, and for illustration purposes only, the linear regression curve also is included in the figure. The linear, quadratic, and cubic regression models are given by the following expressions (Equations 3, 4, and 5):

Linear Model

$$T(K) = 219.972 + 0.526\ DC \qquad \text{Eq. 3}$$

Quadratic Model

$$T(K) = 209.831 + 0.834\ DC - 0.00133\ DC^2 \qquad \text{Eq. 4}$$

Cubic Model

$$T(K) = 206.127 + 1.0545\ DC^2 - 0.00371\ DC + 6.606E\text{-}6\ DC^3 \qquad \text{Eq. 5}$$

Both quadratic (Eq. 4) and cubic (Eq. 5) models may be used to convert the TM-5 thermal IR band digital counts into radiant temperatures. However, depending upon the range of temperatures in question, one or the other model (either the quadratic or the cubic model) will better fit the actual data, as reported by Bartolucci et al[12].

Temperature Mapping of Water Bodies

To test the TM-5 thermal IR data calibration procedure, a Landsat-5 TM scene (ID: 50139-16035) collected on July 18, 1984 over the Chicago-Illinois, region was utilized. First, a hierarchical classification was performed using data from the 1.55 m to 1.75 m middle IR band to separate the water pixels from all other ground cover types. Then, the relative thermal IR spectral response (digital counts) corresponding to water pixels was calibrated using Equations 3, 4 and 5. The resulting radiant temperatures of water were compared with reference temperatures measured at seven different locations (five in Lake Michigan, and two in the Dresden nuclear power plant cooling lake). Table 7 shows the radiant temperatures computed using the linear, quadratic and cubic models, the original digital counts, the reference temperatures, and the radiant temperatures obtained from the integration of Planck's equation without using regression fits.

In Table 7 notice that the cubic model results show a better fit for the actual data or no-model temperatures, for a temperature range between 16.4° and 30.2° C. Also the radiant temperatures (no-model temperature column) and the reference temperatures (ground temperature column) show a discrepancy in absolute values from a minimum of 0.3° C in Lake Michigan, up to 2.4° C in the Dresden cooling lake. These discrepancies are to be expected because in this thermal IR data calibration procedure the atmospheric effects have not been taken into consideration.

Furthermore, the reference temperatures were obtained a few hours before and after the Landsat-5 TM sensor colleted the thermal IR data. Nevertheless, these preliminary results indicate that there is great potential for utilizing the relatively high spatial resolution thermal IR data from the Thematic Mapper sensors for measuring and mapping earth surface temperatures with a high degree of accuracy and reliability.

Additional analyses of TM-5 thermal IR data in conjunction with more reliable measurements of reference temperatures and use of atmospheric effects correction models should be conducted before a final verdict is given for the Landsat TM thermal IR data collection capabilities.

Summary and Conclusions

This paper describes results of Landsats 4 and 5 sensor data quality analysis activities which were carried out over a three-year period covering the Landsat 4 and 5 launches and deployment. The geometric and radiometric errors found in the TM-5 data were not large and their effect on utilization of the data is considered to be small. The performance must be considered in terms of original specifications. For geometry, two parameters are most significant: band-to-band registration and large area geometric fidelity. Band-to-band registratin tests indicate that all bands are within or near specification. Large area geometric accuracy evaluation is not reported in this paper.

Radiometric analysis indicates that some striping and scan-direction dependent banding still exists but with small amplitude. Banding is most severe in Band 4 with nominally a one-count difference between east and west scans. Several coherent noise frequencies still exist in the data; however, they are also of low amplitude. The total energy in these frequencies is very small; no known effects on data utility are expected.

Resolution estimation of TM-5 detectors produced results similar to TM-4 with IFOV values slightly larger than the specifications. This is expected to be due to a combination of smoothing because of processing effects plus atmospheric effects. Thermal calibration activities produced a method for obtaining a temperature for each digital count for TM-5.

References

1. Malaret. E. 1984. "Methods for the determination of the PSF and restoration of images in the Landsat-D Thematic Mapper." Ph.D. Thesis. Purdue University, School of Electrical Engineering, West Lafayette, IN 47907.

2. Rosenfeld, A., A. Kak. 1982. Digital Picture Processing, Vol. 2, 2nd ed., Academic Press, New York, NY.

3. Application notice for participation in the Landsat-D Image Data Quality Analysis Program, Oct. 23, 1981.

4. Anuta, Paul E., Luis A. Bartolucci, M. Ellen Dean, D. Fabian Lozano, Erick Malaret, Clare D. McGillem, Jose A. Valdes, Carlos R. Valenzuela. 1984. "Landsat-4 MSS and Thematic Mapper data quality and information content analysis." IEEE Trans. Geosci. and Remote Sens. GE-22(3):222-236.

5. Bernstein, R., et al. 1984. "Analysis and processing of Landsat-4 sensor data using advanced image processing techniques and technologies." IEEE Trans. Geosi. and Remote Sens. GE-22(3):192-221.

6. McGillem, C.D., P.E. Anuta, E. Malaret, and K.B. Yu. 1983. "Estimation of a remote sensing system point-spread function from measured imagery." Proc. 9th Intl. Symp. on Mach. Proc. Remotely Sensed Data, LARS/Purdue University, West Lafayette, IN, June 21-23, 1983, pp. 62-68.

7. McGillem, C.D., E. Malaret, P.E Anuta. 1984. "Resolution estimation for the Landsat-4 Thematic Mapper." Proc. Conf. Techniques for Extraction of Information from Remotely Sensed Images, Society of Photographic Scientists and Engineers, Springfield, MD.

8. Hughes Aircraft Co. 1985. Personal communication excerpted from a paper by Jack C. Lansing and John Barker, Feb. 18, 1985, Goleta, CA.

9. NASA, 1093. 1983. Interface Control Document between NASA Goddard Space Center (GSFC) and Dept. of Interior, EROS Data Center (EDC) for Landsat-D, Computer Compatible Tape (CCT-AT, CCT-PT), NASA/Goddard Space Flight Center, Greenbelt, MD 20771, Rev. A, LSD-ICD-105, Dec. 1983.

10. Markham, B.L., J.L. Barker. 1985. "Spectral Characterization of the Landsat Thematic Mapper Sensors," NASA Conf. Publication 2355, Vol. II--Thematic Mapper (TM), Part 1, pp: II-235 - II-276.

11. Bartolucci, L.A., R.M. Hoffer, T.R. West. 1973. "Computer-Aided Processing of Remotely Sensed Data for Temperature Mapping of Surface Water from Aircraft Altitudes," LARS Technical Report 042373, LARS/Purdue Univ., West Lafayette, IN, 47906-1399.

12. Bartolucci, L.A., P.E. Anuta, D.F. Lozano. 1985. "Evaluation of TM-5 Thermal IR Band Radiometric Calibration for Water Temperature

Mapping " Proc. 11th Intl. Symp. Mach. Proc. of Remotely Sensed Data, LARS/Purdue Univ., West Lafayette, IN, June 25-27. (In press)

LIST OF TABLES

Table 1. Misregistration in the across-track direction over a 256x64 block in Illinois.

Band		1	2	3	4	5	7	6
1		0.00	0.00	0.00	0.06	0.04	0.02	0.32
2			0.00	0.00	0.07	0.02	0.01	0.45
3				0.00	0.06	0.02	0.01	0.49
4	$[X_{ij}] =$				0.00	-0.02	-0.02	-0.30
5						0.00	-0.01	0.04
7							0.00	-0.32
6								0.00
1		0.00	0.06	0.07	0.21	0.16	0.14	2.76
2			0.00	0.02	0.19	0.11	0.12	2.71
3				0.00	0.12	0.08	0.10	2.68
4	$[\sigma_{X_{ij}}] =$				0.00	0.12	0.08	1.70
5						0.00	0.07	1.85
7							0.00	1.62
6								0.00

Table 2. TM-5 misregistration in the along-track direction over a 64x256 block in Illinois.

Band		1	2	3	4	5	7	6
1		0.00	0.01	0.01	-0.06	0.07	0.06	0.36
2			0.00	0.01	0.00	0.05	0.04	0.67
3				0.00	-0.01	0.02	0.01	0.40
4	$[X_{ij}] =$				0.00	0.05	0.06	0.14
5						0.00	-0.01	0.00
7							0.00	-0.25
6								0.00
1		0.00	0.03	0.02	0.53	0.17	0.15	1.85
2			0.00	0.02	0.23	0.12	0.11	1.82
3				0.00	0.07	0.10	0.09	2.01
4	$[\sigma_{X_{ij}}] =$				0.00	0.19	0.12	1.89
5						0.00	0.03	1.79
7							0.00	1.31
6								0.00

Table 3. Coherent noise periods (in pixel cycle) using Lake Michigan data.

Band	TM-4	TM-5
1	17, 3.12	none
2	17, 3.12	6.24
3	17, 3.12	12.8, 6.24, 5.12
4	17, 3.12	5.12
5	3.12 hardly noticeable	5.12
7	3.12 hardly noticeable	12.19, 5.12
6	none	none

Table 4. Results of TM resolution estimation in terms of half-amplitude width.

Band	Trig. Smoothing, W1/2(si)	Spline Smoothing, W1/2(si)
1	1.42 si	1.25 si
2	1.20 si	1.16 si
3	1.42 si	1.31 si
4	1.50 si	1.06 si
5	1.33 si	1.34 si
7	1.37 si	1.49 si

si = sampling interval

Table 7.

Temperature for Models of Range 203.2 - 341.2 K, Landsat-5.

Site	Digital Counts	Linear C	Quadratic C	Cubic C	Ground Temp.	No Model Temp.
CHICAGO						
Foster	121.8	10.9	18.6	18.3	17.2	17.5
Montrose	121.8	10.9	18.6	18.3	16.1	17.5
North Ave	119.5	9.7	17.4	17.2	16.7	16.4
Oak st.	126.0	13.1	20.8	20.1	17.8	19.4
Calumet	126.1	13.1	20.8	20.2	17.8	19.5
DRESDEN NUCLEAR POWER PLANT						
Spillway	142.0	21.5	28.4	26.8	28.8	26.4
Bridge 4	151.0	26.2	32.4	30.3	32.2	30.2

LIST OF FIGURES

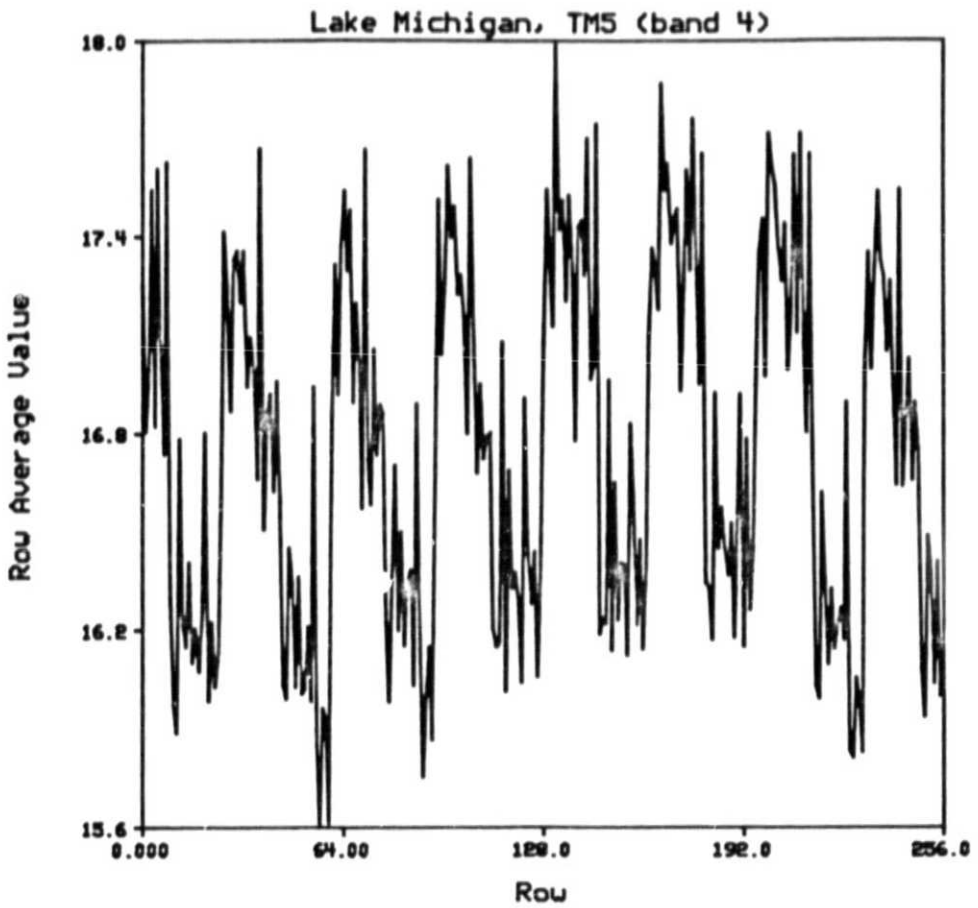

Figure 1. Scan-line averaging for low-level TM-5 Band 4 data over a 256x256 block showing scan-to-scan striping.

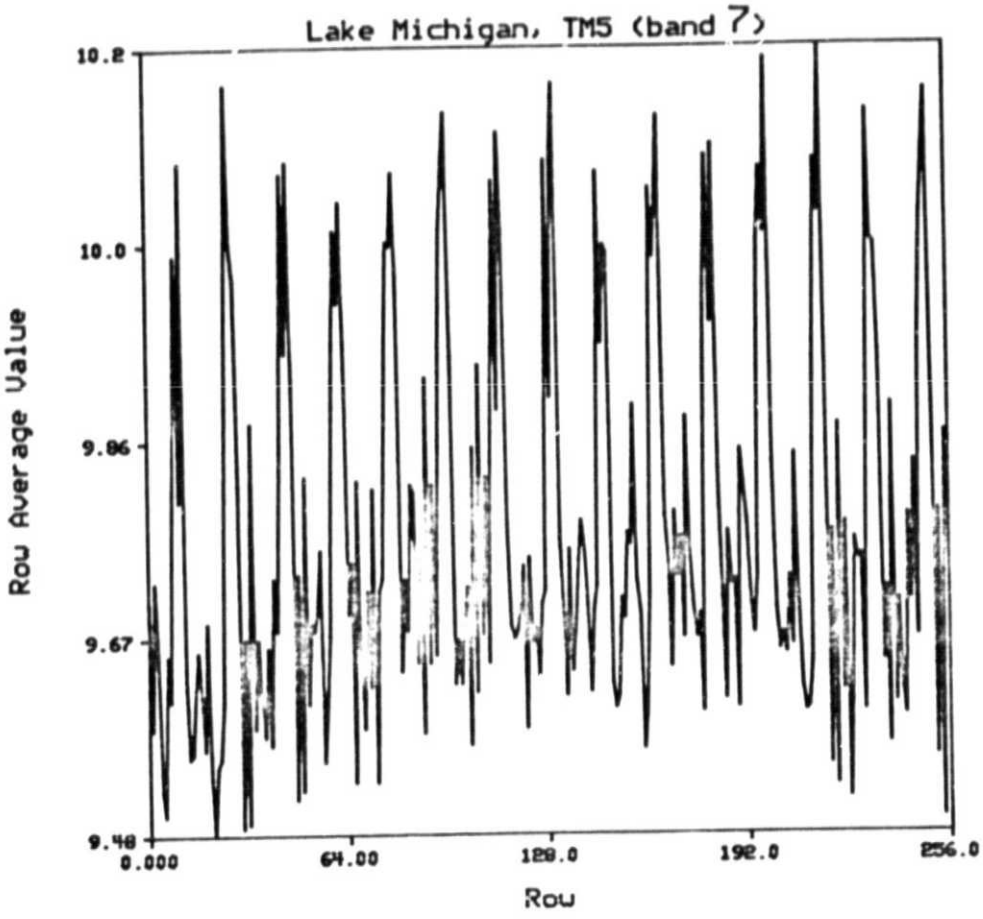

Figure 2. Scan-line averaging for low-level TM-5 Band 6 data over a 256x256 block showing detector-to-detector striping.

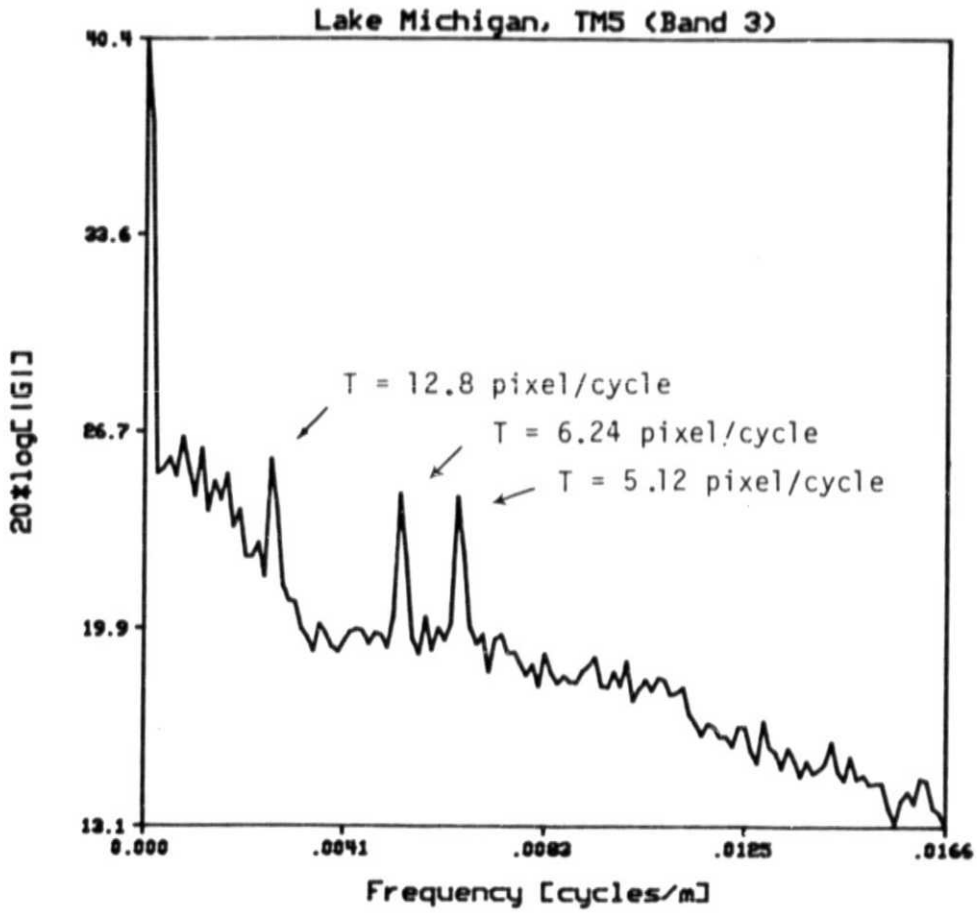

Figure 3. Power spectrum of low-level TM-5 data showing noise peaks at = 5.12, 6.24, 12.8 pixel/cycle.

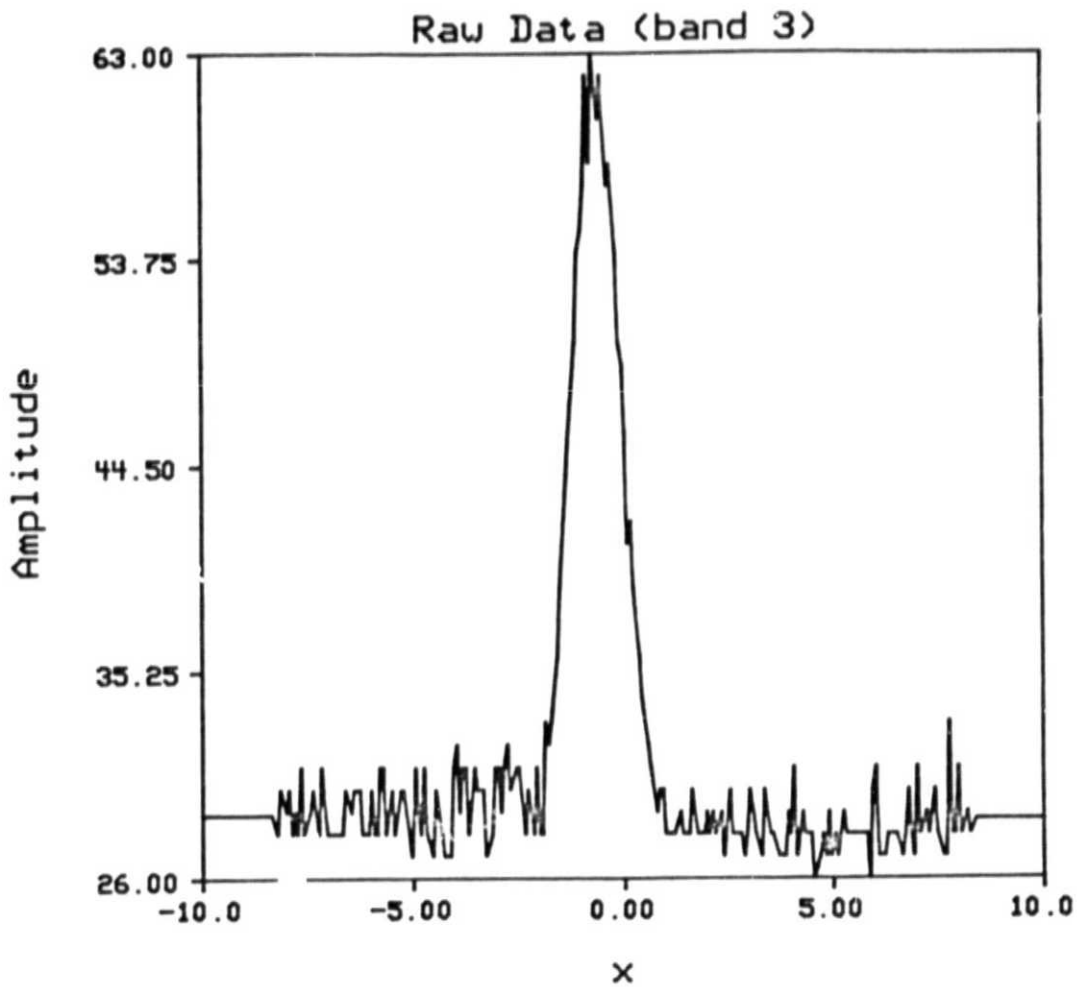

Figure 4. Extracted road raw data from rural area in Illinois.

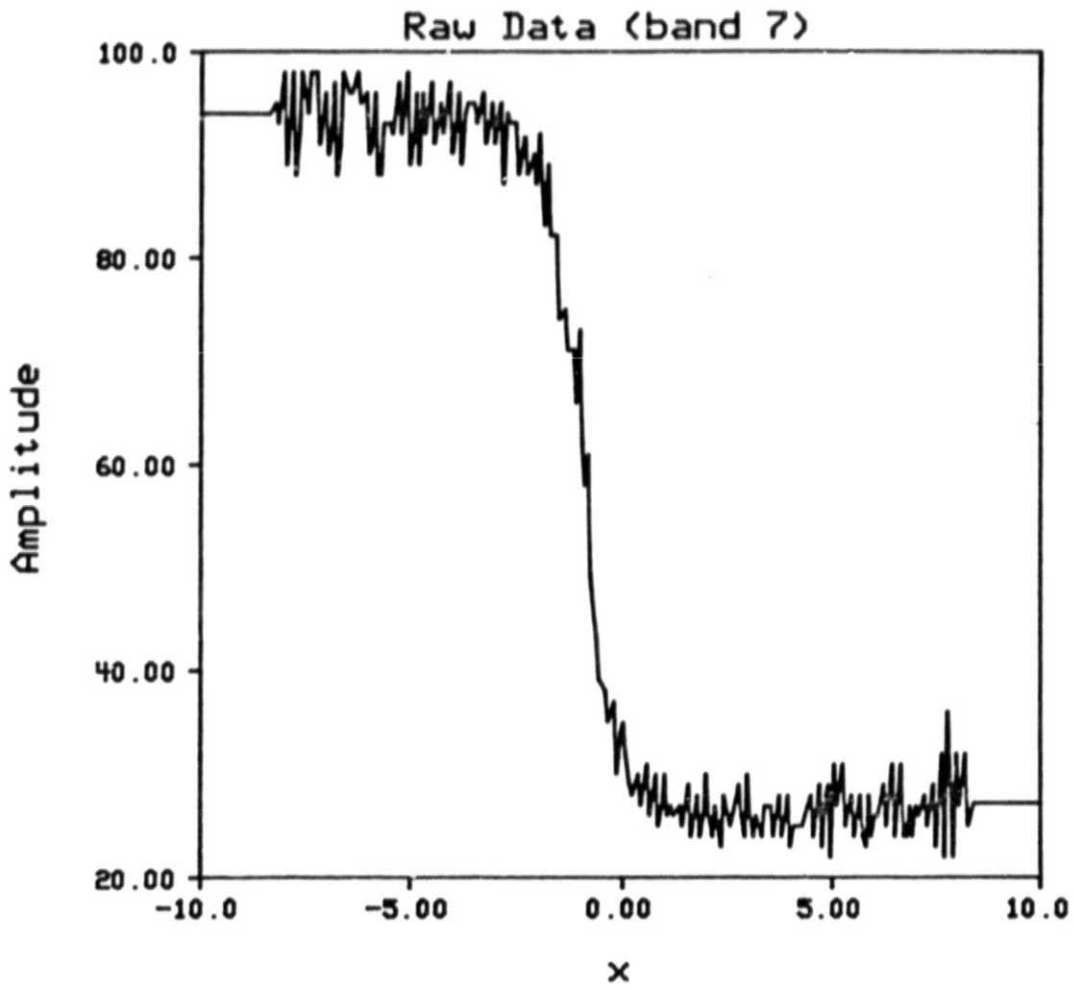

Figure 5. Extracted step edge raw data from Illinois scene.

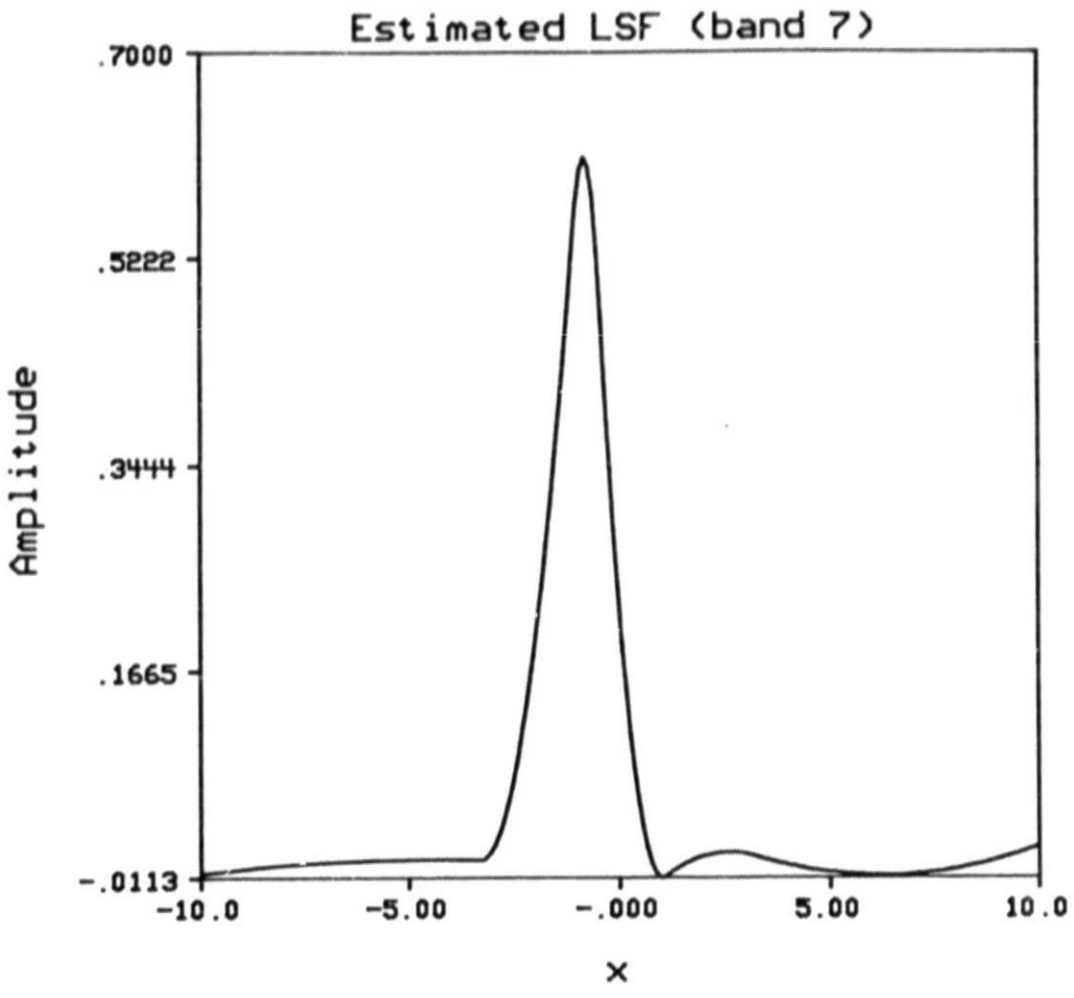

Figure 6. Estimated LSF from step edge for TM-5 Band 7.

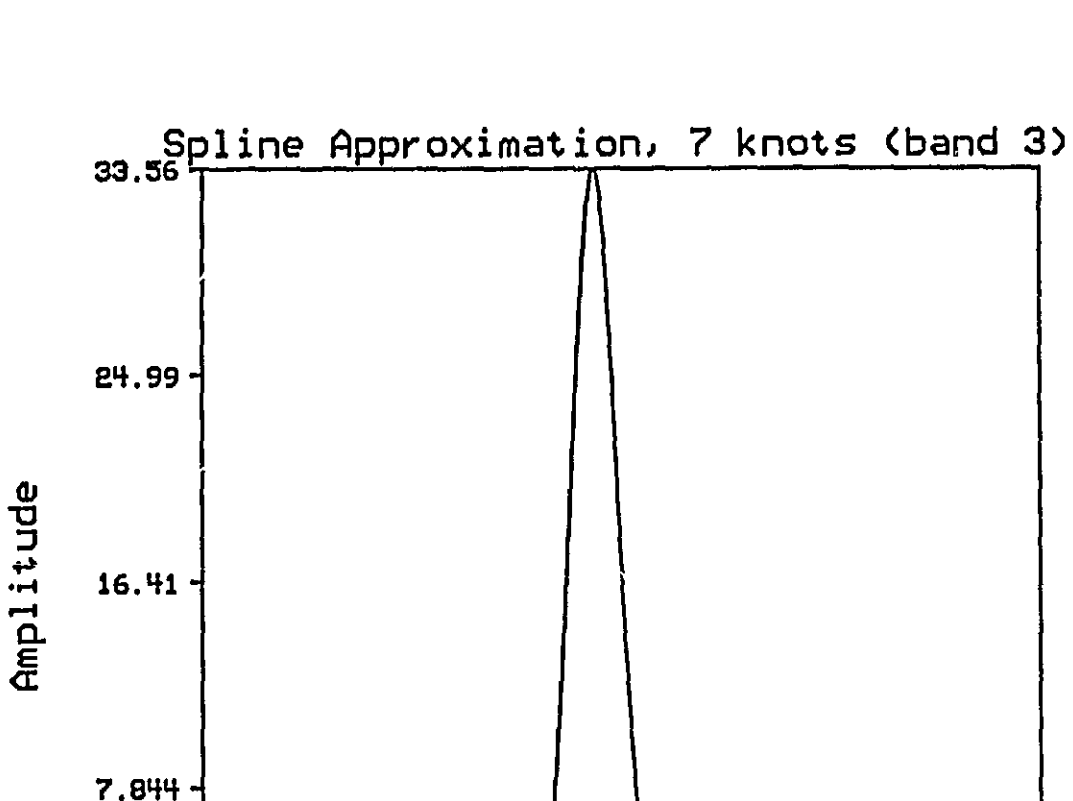

Figure 7. Estimated LSF from the system response to a road for TM-5 Band 3.

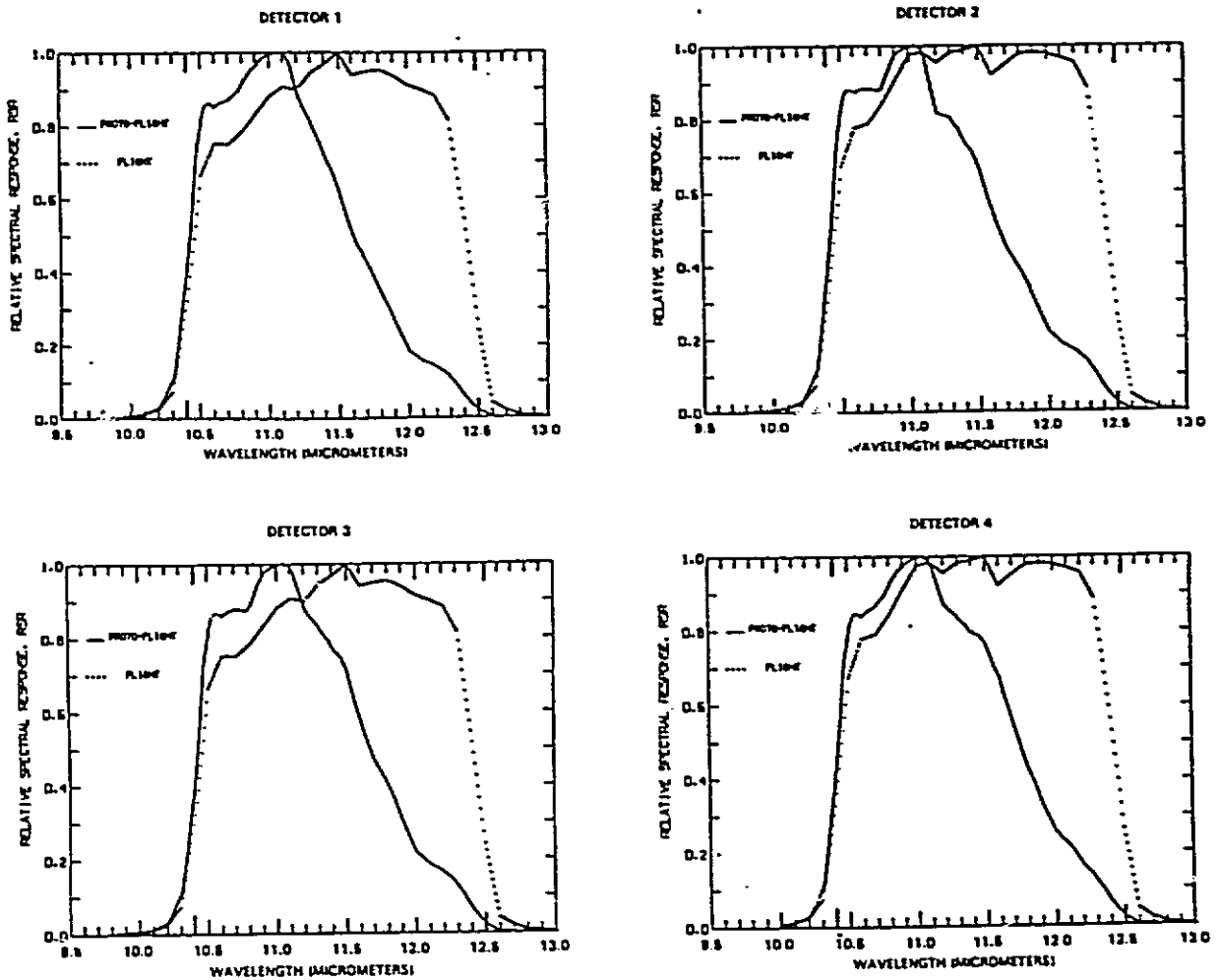

Figure 8. System Response Curves for the Landsat-4 (Proto-Flight) and Landsat-5 (Flight) Thermal IR Band Detectors. [After Markham and Barker, 1985]

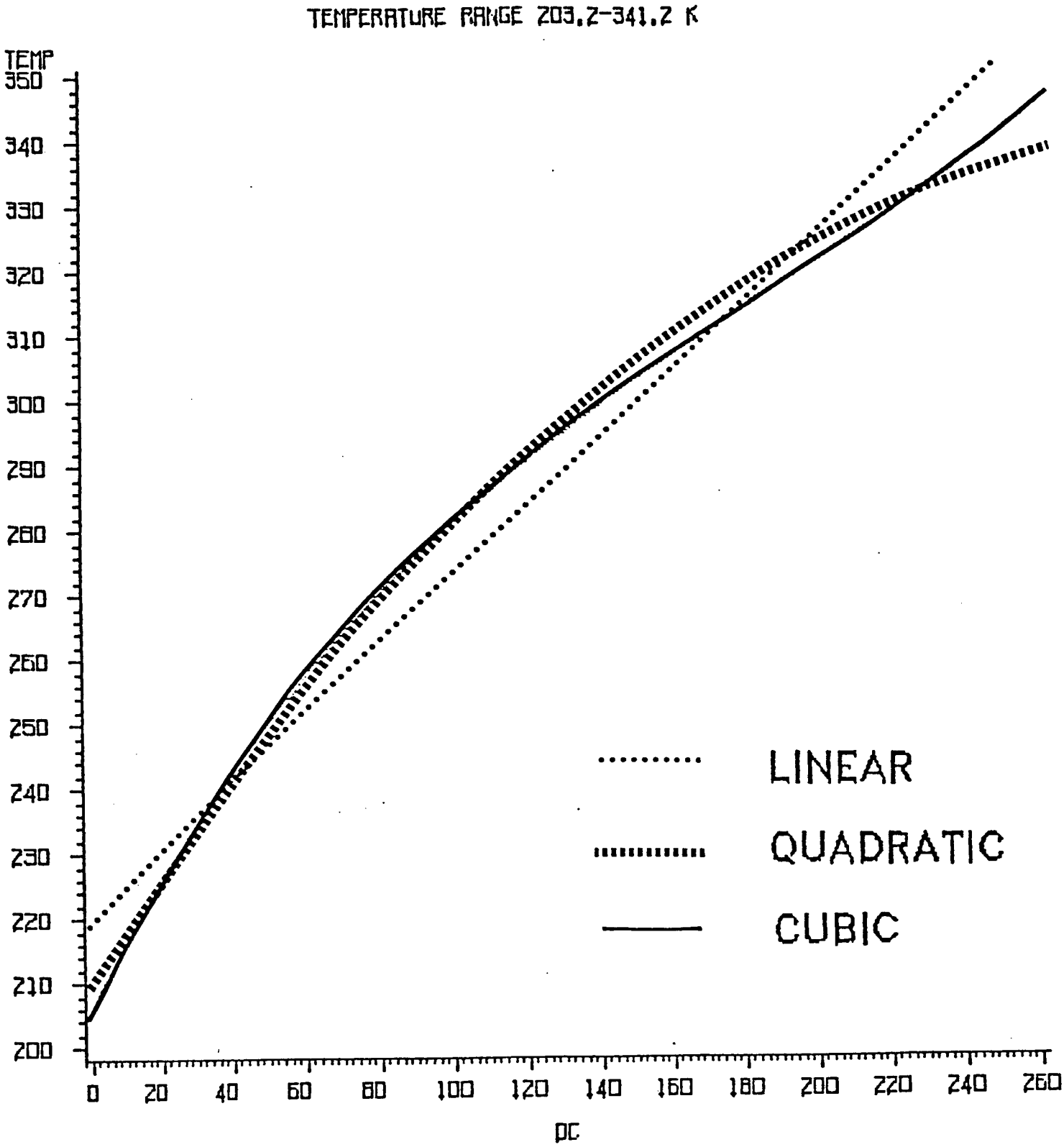

Figure 9. Linear, Quadratic and Cubic Regression Models for the Relationship Between Digital Counts and Temperature for the Landsat-5 TM Thermal IR Band.

APPENDIX

Landsat-4 MSS and Thematic Mapper Data Quality and Information Content Analysis

by

P. Anuta, L. Bartolucci, E. Dean
F. Lozano, E. Malaret, C. McGillem
J. Valdes, C. Valenzuela

Laboratory for Applications of Remote Sensing
Purdue University
West Lafayette, IN 47906-1399

Abstract

Landsat-4 thematic mapper and multispectral scanner data were analyzed to obtain information on data quality and information content. Geometric evaluations were performed to test band-to-band registration accuracy. Thematic mapper overall system resolution was evaluated using scene objects which demonstrated sharp high contrast edge responses. Radiometric evaluation included detector relative calibration, effects of resampling, and coherent noise effects. Information content evaluation was carried out using clustering, principal components, transformed divergence separability measure, and numerous supervised classifiers on data from Iowa and Illinois. A detailed spectral class analysis (multispectral classification) was carried out on data from the Des Moines, Iowa area to compare the information content of the MSS and TM for a large number of scene classes.

Introduction

Landsat-4 thematic mapper and multispectral scanner data were analyzed in this study to obtain information on data quality and information content. Geometric evaluations were performed to test band-to-band registration accuracy. Thematic mapper overall system resolution was evaluated

---

* This work is sponsored by the National Aeronautics and Space Administration under NASA Contract NAS5-26859.

using scene objects which demonstrated sharp high contrast edge responses. Radiometric evaluation included detector relative calibration, coherent noise analysis and the effects of resampling. Information content evaluation was carried out using clustering, principal components, and the transformed divergence separability measure on data from Iowa and Chicago, Illinois. A detailed spectral class analysis (multispectral classification) was carried out on data from the Des Moines, Iowa area to compare the information content of the MSS and TM for a large number of scene classes. This work is being carried out as part of a Landsat-4 data quality evaluation study.

Test Data Sets

The data sets used in this study were gathered over the Des Moines, IA area on Sept. 3, 1982 and the Chicago, IL area on October 25, 1982. Both A tapes which are radiometrically corrected and P tapes which are both radiometrically and geometrically corrected were acquired for these scenes. The scene numbers were 40049-16264 for Iowa and 40101-16025 for Illinois. Preliminary test scenes over Detroit and Arkansas were also available.

Comparison of A and P Tape Data

To determine the effect of the geometric correction process (resampling and gray-level interpolation) on the radiometry of the new resampled pixels when converting the data from an A-tape (30m x 30m pixels) to a P-tape (28.5m x 28.5m pixels) format, the means and standard deviations for homogeneous and heterogeneous areas on the ground were calculated using the data from both the A and P tapes. A qualitative comparison of both sets of statistics indicated that no change (radiometric degradation) was caused by the non-zero order (cubic convolution) interpolation process.

Furthermore, to determine whether the cubic convolution interpolation had affected the structure of the data in feature space, a set of data from the A and P tapes for the same area on the ground was clustered into 16 cluster classes. Then the resulting 16 cluster classes from the A and P-tape data sets were merged together into a single 32-class file. Subsequently, the pair-wise spectral separability for the 32 classes was computed using a Transformed Divergence algorithm[1]. The minimum transformed divergence between cluster classes from the TM A tape and corresponding second cluster classes from the TM P tape is 22 and the maximum is 262. Since the transformed divergence (D_T) measure ranges from zero to 2,000 -- where a value of 2,000 indicates that the two classes in question are completely separable (different) and any D_T value between zero and 500 indicates that the pair of classes is not separable (very similar) -- it may be concluded that the 16 cluster classes obtained from the A and P tapes are essentially equivalent. Thus, these results corroborate the previously stated conclusion that the radiometry of the resampled pixels from the P tape has not been significantly affected by the geometric correction process. Consequently, they meet GSFC specifications for the Landsat-D system, i.e., resampling shall not introduce radiometric degradation of more than 1 quantum level[2].

Registration Evaluation

The first TM scene, which was of the Detroit area, contained several geometric and radiometric errors which did not appear in subsequent scenes. The overall visual quality of TM data is extremely good; detailed analysis is required to find subtle errors. Band-to-band registration was evaluated using a correlation algorithm capable of estimating shifts to subpixel

accuracy. The algorithm implements the correlation coefficient and user cubic interpolation to estimate the peak to subpixel accuracy. The means and standard deviations of shifts for 32 sets of lines in TM imagery of the Iowa and Arkansas sites were computed. Results indicate that the primary focal plane bands (1, 2, 3, 4) are registered to .1 pixel, which is well within the .2 pixel specification. Bands 5 and 7 are also well registered to within the .2 pixel specification.

Problems were discovered, however, in the registration of the first band set (1, 2, 3, 4) to Bands 5 and 7. Approximately .6 pixel misregistration was observed between these bands, which exceeds the specifications of .3. The thermal IR band could not be numerically correlated due to the great difference in the nature of the image relative to any of the other bands, so a visual blink comparison was used on a digital display unit. A four 30 M pixel line misregistration was observed in both Arkansas and Iowa thermal data.

The MSS band-to-band registration was similarly evaluated and shifts were found to be less than the .2 pixel tolerance for the A data, but slightly greater than the tolerance for P data. The maximum shift of .27 was between Bands 1 and 2.

Detector-to-Detector Calibration

Thematic mapper detector-to-detector calibration was evaluated by computing mean values of sets of scan lines spaced 16 lines apart in A-tape data. Results are presented in Table 1. Differences as large as 1.3 digital count were observed, but the typical deviations from the overall mean were less than .5 digital count. These results indicate that striping should be minimal in TM data. This is verified by visual inspection of the imagery.

Similar tests were run on MSS data. The results are presented in Table 2 in terms of maximum deviation from overall means and variances. The values are all below one bin, indicating that relative calibration is very good.

Coherent Noise Analysis

Visual inspection of MSS imagery over Lake Michigan revealed significant noise patterns in all bands. These wavelike patterns had a period of 14 to 15 samples with higher frequency patterns superimposed. The magnitude of the noise is 4 to 5 counts peak-to-peak and it exists in all bands. It was first assumed that this noise was a jitter effect. Fourier analysis was performed on samples of the noise patterns and several significant frequencies were observed. The largest had wavelengths of 3.31, 4.09 and 15.4 pixels which agreed with the visual inspection. The frequencies were all too high, however, to be caused by jitter. A sampling, power supply, or data processing is suspected as the cause.

No visual noise effects were apparent in the thematic mapper data. However, Fourier analysis of low level Lake Michigan data revealed two coherent noise frequencies in some of the bands. Figure 1 contains a plot of the power spectrum of data from band 4 detector 1 and two noise frequencies are apparent. One is at a wavelength of 17 pixels and the other is at 3.12 pixels. The power in these frequencies is 10 to 20 decibels (10 to 100 times) above the background noise level, but relative to the power in the bright areas of the scene the noise power is very low. The amplitude of the 3.12 pixel noise signal is 24 decibels and the low frequency power in the Sept. 23, 1982 Iowa TM data is in the 60 decibel range, thus the noise is more than 30 decibels less than the image power. This corresponds to a

standard deviation of nominally 30 times less than the signal. Band 4 standard deviation is 21 counts for typical sites in the Iowa data, thus the amplitude of the noise is nominally 0.6 count. These noise frequencies exist in all detectors of band 4. This noise was observed in bands 1,2,3 also, but not in bands 5,6 and 7.

The MSS and TM noise frequencies are nominally the same suggesting a common cause, but no explanation is advanced here. These results are presented as evidence to aid researchers and data processing agencies in correction and refinement of the sensor and data processing stream to aid in assuring maximum quality of Landsat-4 data.

Resolution Estimation in TM Data

One geometric parameter of particular interest is the actual in-flight resolution of the sensor system which includes all environmental and data processing factors. The resolution is determined by the point-spread function (PSF) of the system. This can be estimated in image data by observing the measured response to scene elements of known shape.

The measured data can be expressed in the spatial domain as a convolution of the scene with an overall point-spread function:

$$g(x,y) = h(x,y) * f(x,y)$$

where $f(x,y)$ is the earth scene

$h(x,y)$ is the overall point-spread function of the sensor system

$g(x,y)$ is the resulting image

Given g(x,y), we wish to determine h(x,y). To do this, some deterministic element of the input f(x,y) must be known or assumed. Although the theory can take into account the two-dimensional nature of the element, the initial experiments have been limited to the one-dimensional case. If the overall PSF is separable, i.e., if h(x,y) can be written as a product h(x)h(y), then this approach provides a direct estimate of the two components. Otherwise it generates cross sections through the two-dimensional PSF along the x and y axes.

Three scene elements that would be useful for this type of analysis are:

1. An impulse represented by a narrow-width discontinuity along a row or column of the data.

2. A step function represented by an abrupt change in gray level along a row or column of the data.

3. A rectangular pulse represented by a sequence of two steps in opposite directions along a row or column of the data.

It was observed by experimentation with the three types of scene elements that the step edge was the most desirable to use. In particular, agricultural field edges for high contrast fields with uniform texture were used. To determine the PSF, subpixel sampling is required since the sample rate of the sensor is nominally the width of the PSF. A procedure was defined to allow subpixel sampling of edges.

Because of the orbital inclination of Landsat and the propensity of man to arrange linear features, such as roads and field boundaries, in the cardinal compass directions, it is generally found that there is a spatial

displacement in the scene coordinates of the linear elements from one row or column to the next. This has the desirable effect of providing a fine grid of samples of the system response when values from adjacent rows or columns are combined after correction for the spatial shift of the scene element. The procedure for combining the data is quite straightforward and can be illustrated as follows for a north-south road.

The coordinates of the peaks in the row data corresponding to the road are determined for a sequence of N rows. These data are then fitted with a least-squares straightline, providing an analytical expression for the road coordinates. The x-coordinates in each row are then modified by subtracting from them the least-squares estimate of the road location in that row. This converts the data to a coordinate system in which zero is the road center. Because of the small angular difference between the sensor coordinate system and the road direction, the change in road coordinates from row to row is only a fraction of the pixel spacing and so represents a sampled response to the scene element corresponding to a subpixel translation. By combining the data from a number of rows, a set of finely sampled data is found. These data can be graduated using splines or other smoothing functions to give an average response function from which to estimate the system point-spread function.

The subpixel sampling scheme was applied to field edges in the Iowa data set. A dense set of samples was obtained for several edges in TM Bands 4 and 5. The PSF was estimated in earlier work[3] using a finite sum of basis functions. The method used here is based on the following observations:

The scene element can be modeled as a step superimposed on a constant background, i.e.,

$$f(x) = A + B\,u(x)$$

where A is the background and B is the amplitude change across the boundary. The output is then given by

$$g(x) = [A + B\,u(x)] * h(x)$$

Taking the derivative of both sides of this equation gives

$$g'(x) = (A+B\,u(x)) * h(x)$$

$$= B\,\delta(x) * h(x)$$

$$= B\,h(x)$$

$$h(x) = g'(x)$$

The PSF is therefore the derivative of the measured step function. The measured subpixel sampled step data were smoothed to produce a well-behaved derivative. If this had not been done, the derivative would have been excessively noisy. Two methods of smoothing were used: (1) Trigonometric polynomials, and (2) cubic spline functions [4].

A simulation experiment was conducted using an ideal edge with Gaussian noise to test the smoothing methods. A test PSF was convolved with the noisy edge and the result was smoothed and the PSF width was determined by differentiation. It was observed that the spline smoothing tended to underestimate the width by 10% and the trigonometric smoothing overestimated by 15%. The results were used as correction factors when the method was applied to real data.

Field-edge data for two cases were extracted from the Iowa scene and the derivative PSF estimation scheme was applied. The resulting estimated point spread function for Band 4 is shown in Figure 2. The results for the two types of smoothing are listed in Table 3. The width measure is the half amplitude of the estimated PSF. These results indicate that the actual overall resolution is less than the optical system resolution. This would be due to atmospheric and data processing effects or to the characteristics of the field edge. The effect of smoothing may also be significant but the simulation experiment provided a correction which is believed to compensate for this. These results are based on a limited sample under one atmospheric state and further estimation research must be carried out to determine the variability of the resolution estimates.

Scan Angle Effects

The effect of scan-look angle on the recorded digital response value was studied using the TM A Tape from Iowa (Scene ID:40049-16264). Average digital values calculated from 3 blocks each of dimensions 16 lines (detector) by 10 columns were obtained for both the forward and reverse scans; each set of 3 blocks was selected at intervals of 100 columns for each of the reflective bands. Figure 3 shows a plot of the average digital response values for the forward and reverse scans for Band 1. This figure shows a general decline in average response across-track, with a total drop of about 4 to 5 digital counts. Some of the other channels displayed similar, although somewhat lower and less distinct drops in digital counts across-track. Much of the variance across-track was due to scene variation and both linear and multiple regressions failed to produce significant equations for all bands (Table 4), but a general decline in response does seem

to exist for some if not all of the bands, as indicated by a negative slope obtained for all regressions from both reverse and forward scans for all bands. No significant difference between the forward and reverse scans for any band was found for the Iowa TM A Tape using an alpha level = 0.05.

Dimensionality of TM vs. MSS

The spectral dimensionality of the TM sensor is of great interest since it potentially represents nearly double the information over the MSS. The dimensionality was investigated by applying the principal components transformation to test data.

One of the major advantages of using orthogonal linear transformations, such as the Principal Component or Karhunen-Loeve transformation, is their ability to compress overall data variance in a multifeature space onto a relatively few transformed orthogonal axes. This essentially separates non-random variance (information content) from random variance (noise) while, concurrently, uncorrelating the transformed axes in such a way that any information redundancy (due to interband correlation) is eliminated. Such transformations therefore allow a compression of the data into a fewer number of dimensions while retaining a maximum amount of significant information content and removing much of the random variance or noise from the data.

Principal components were generated for both the MSS and TM P-tape data sets from the Chicago O'Hare test site. Statistics used in calculating the principal components were generated from data samples of the original MSS and TM data sets from every fifth line and fifth column and all bands. Since the sum of the eigenvalues is equal to the trace of the original covariance matrix, i.e., the total variance, the importance or percent of total variance explained by eigenvector(λ_1) is given by:

$$\frac{\lambda_1}{\text{tr } S}$$

where λ_1 = eigenvalue i or characteristic root of the ith component

tr S = trace of covariance matrix S or total variance.

Therefore, each of the eigenvalues of the ordered components divided by the sum of the eigenvalues represents the amount of total data variance or information content accounted for by each eigenvector. Tables 5 and 6 list the eigenvalues and the corresponding amount of data variance that is accounted for by their respective eigenvectors for both the MSS and the TM data sets. As shown in these tables, the first two principal components of the MSS P-tape account for almost 97% of the total data variance. This is also evident from the images of the ordered MSS principal components (Fig. 4). The first two components contain a significant amount of scene contrast and data structure, while the last two MSS components contain mostly random noise.

In the TM data set, the first two ordered components together account for 90% of the data variance, the first three account for 97.45%, and the first four components account for almost 99% of the data variance. The images of the TM principal components also show that the first four components contain a significant amount of scene contrast with a sequential decrease in the lower-ordered components (Fig. 5).

From both the listed eigenvalues of the MSS and TM data sets, it is possible to conclude that the first two components of the MSS and the first

four components of the TM data sets contain a maximum amount of significant information. It could be possible, therefore, to conclude that for this data set of the Chicago O'Hare area, the TM data contain more significant information, i.e., a higher significant dimensionality, than the corresponding MSS data set. The significant dimensionality as defined by a principal component analysis may be substantially different for other data sets and other ground cover types. However, these results do imply that for the same area, the TM may contain more significant information than the corresponding MSS.

Principal Component Comparison:

(Chicago O'Hare and Des Moines Iowa TM Data)

In order to investigate both the significant dimensionality and the importance of the individual TM bands for different data sets, a principal component analysis was performed on the Des Moines Iowa TM data (Scene ID:40049-16264) and compared with the principal components analysis of the Chicago O'Hare TM data set discussed above.

Since the coefficients of a particular principal component correspond to the direction cosines of the original bands to the new component [5], it is possible to describe the relative direction of the new component axis in the feature space with respect to the original bands. The greater the coefficient of a particular band to a specific component, the larger the cosine and thus the smaller the angle subtended between the original feature axis (band) and the new component axis, i.e., the more the new component axis lies in the direction of the original feature axis (band). In this way it is possible to describe the relative influence or "pull" of the original bands on each of the new component axes.

Using the coefficients of the higher-ordered principal components, i.e., those components which incorporate most of the total data variance, it is possible to describe which of the original bands contain most of the significant variance or information content for a particular data set. Figures 6 and 7 graphically show the loadings or coefficients of the Chicago O'Hare airport and the Des Moines, IA TM data sets, respectively. In addition, Figure 8 graphically shows the percent of total data variance accounted for by each eigenvector (principal component) of the Chicago O'Hare and Des Moines, IA TM data sets.

It is interesting to compare these two data sets in that they demonstrate the importance of different bands for different data sets of varying cover type. The first eigenvector or component of the O'Hare data set shows relatively equal weighting of all of the original reflective bands (Fig. 6). By comparison, the greater amount of vegetation (primarily agricultural crops and forest areas) associated with the Des Moines TM data set has resulted in a significant amount of the total variance (accounted for by PC1, Fig. 8) of the data to be contained on Band 4 and, to a lesser extent, Band 5. The second component of the Des Moines TM data set contains more information from the rest of the bands. It is interesting to note that component four of both the Chicago O'Hare and Des Moines TM data sets has the greatest contribution from band 6 (thermal IR) (Fig. 6 and 7), which is clearly evident from a comparison of the two images, i.e. component 4 and the original band 6 (Fig. 5). This may imply that although the thermal IR band may not contain a significant amount of total data variance (the fourth component of both data sets describe only 1-2% of the total data variance), the information or variance may be distinctly unique from the

rest of the bands. In addition, although most of the significant variance was incorporated on different bands for these two data sets (as described by the first eigenvector for each set), both sets indicate a significant dimensionality of between 3 and 4 dimensions (Fig. 8).

Spectral Class Analysis in TM and MSS Data

A detailed spectral analysis was conducted of thematic mapper and MSS data for an area near Des Moines, Iowa from the September 3, 1982 data set. Data were utilized from 7 blocks distributed throughout the area which included agricultural, forest, suburban, urban, and water scene types. The blocks were processed using a clustering algorithm to produce up to 18 cluster groupings for each block. Each cluster class was then identified with a ground-cover class using aerial photography and maps of the area. The cluster classes from each of the 7 blocks were inspected with regard to separabililty, means, variances, and number of points in each class were either deleted or pooled with spectrally similar clusters[19]. The separability measure used in the transformed divergence function or processor [6] measures the statistical distance between classes based on class means and covariance matrices. The measure has a maximum value of 2,000 and the minimum of 0. Spectrally, very close classes will typically have values as low as 50 to 500.

For the TM data, initially 94 classes were defined and the pooling and deleting process reduced these to 42 final spectrally separable classes. Table 7 lists these classes. The MSS data were then analyzed using the same clustering and merging sequence. The number of separable classes in the MSS is 21, half of the TM result. This result is considered to be a very significant indicator of the dimensionality of TM relative to MSS.

The MSS class occurrences are indicated in Table 7. The maximum divergence values of any one class with respect to all others also were much less for the MSS classes relative to TM. Table 8 contains the maximum and average transformed divergence values for the 42 spectral classes and for the best subsets of TM spectral bands. It should be noted that the best spectral band for any combination of Bands 1 through 7 is the first middle IR band (1.55-1.75μm). The next best band is the near IR (0.76-0.90μm), followed by the red band and then the thermal IR. The best combination of four bands includes one from each of the four regions of the spectrum (visible, near IR, middle IR, and thermal IR). Table 9 contains the minimum and average transformed divergence values for the best combination of MSS bands.

The high average divergence indicates that the 21 spectral classes found in the MSS were about as separable as the TM classes. However, there was twice the number of equally separable TM classes. This is considered to be the most significant result of the spectral analysis.

A final test using a preliminary set of test data was carried out using the small amount of ground truth available. A set of 5,615 TM and 1,376 MSS pixels containing forest, corn, soybean, soil, water, and urban classes was extracted from the TM and MSS data where the cover classes were known or could be inferred from aerial photography. The overall correct recognition was 95.7% for the TM classification using all 7 bands, 92.6% for the TM using a subset of the best four bands, and 67.4% for the MSS classification using all 4 bands and a per-point, Gaussian Maximum Likelihood (GML) classifier. The results are listed in Table 10 along with the amount of CPU time required to classify each data set.

An additional classification using all 7 TM bands was performed on the test data using a contextual algorithm, SECHO (Supervised Extraction and Classification of Homogeneous Objects), in order to demonstrate the effectiveness of such contextual algorithms over per-point algorithms for use with the 30 meter resolution TM data. The contextual or per-field algorithm SECHO first divides the scene to be classified into homogeneous fields and then classifies these fields using an extension of the GML algorithm [7]. SECHO incorporates the fact that since cover classes are more likely to occur in homogeneous areas larger than one pixel in size (i.e. larger than 30 meters), adjacent pixels are highly correlated, with the degree of correlation diminishing with an increasing distance between the pixels [7]. Thus SECHO assigns an analyst-specified threshold value, below which adjacent pixels will be grouped into a homogeneous field. Statistics for these fields are calculated and compared to the original cover class statistics and a "homogeneous field" is classified as a unit into that class which it most closely resembles.

These "test" fields are limited in number of pixels and so are not really evaluating how representative the final spectral classes are of the entire scene but rather how separable the classes are. Deletion of certain spectral classes (e.g., Corn2), due to low separability, resulted in much confusion of corn with trees in the MSS but not the TM for both the best four and for all seven TM bands. Also, the resolution of TM actually allowed "purer" cluster classes to be defined since smaller areas (e.g., beaches, roads) were distinct. These results along with the listed CPU time for classification indicate that a subset of the best four TM bands incorporates the advantages of the higher spatial resolution (e.g., "purer"

cluster classes) over the equivalent MSS data without simultaneously incurring as substantial an increase in computer time required for classification as with all seven bands. In addition, these test results support the use of contextual algorithms, such as SECHO, over per-point algorithms for use with TM data. An earlier study using simulated TM data [8] demonstrated that higher classification performances could be expected with the SECHO classifier for the 30 meter TM data, especially in those areas where the cover class field sizes are relatively large, relative to the scanner FOV, e.g., most agricultural areas.

Temperature Mapping of a Cooling Pond and Thermal Plume from a Nuclear Power Plant

The use of thermal infrared (IR) data in conjunction with reflective multispectral data, obtained from aircraft altitudes, has been proven to be an effective means for increasing the classification accuracy of earth surface features [9,10].

Also it has been demonstrated that radiometrically calibrated thermal IR data obtained from airborne platforms can be used to produce accurate temperature maps of water bodies [11,12,13,14].

Accurate temperature maps of water bodies have been obtained also from calibrated thermal IR data gathered in 1973 by the SKYLAB SL-2 S192 scanner system[15]. However, for almost ten years the remote sensing data users have not had available high spatial resolution thermal IR data (in contrast to the coarse spatial resolution data gathered by meteorological satellites) acquired from spaceborne platforms, until the TM thermal data were recently collected.

In order to determine the radiometric quality of the TM thermal data for temperature mapping of surface water, a test site was selected within the area covered by the TM scene (Scene ID: 40101-16025) gathered over Illinois. This site was chosen because it includes a surface water body with a large range of temperatures, i.e. a cooling pond for the Dresden nuclear power plant and the junction of two rivers: the Kankakee and the Des Plaines Rivers which once merged form the Illinois River.

The Dresden power generating station is located approximately 50 miles southwest of Chicago near Morris, Illinois. The station houses three nuclear reactors which together have a maximum nameplate generating capacity of 1,656,630 Kw. The water which is taken from the Kankakee River and is used to cool the stream condensers is channeled into a man-made lake which is designed to dissipate heat. This 1300 acre lake has a dike in its center which directs the water flow up, around, and down the lake in an eight-mile loop that takes two-and-a-half days to complete. During its course the water is cooled by natural evaporation and is either recycled back through the station or discharged into the Illinois River. A schematic diagram of the power plant, channels, cooling lake, and the three rivers is shown in Figure 9.

Because the radiant temperature of the various cover types in the test site is a function not only of the kinetic temperature of the materials, but also a function of the intrinsic emissive properties (emissivity) of the objects, and to avoid differential emissivity complications, it was decided to perform the calibration of the TM thermal IR data corresponding to only those pixels representing water, which has an emissivity close to that of a perfect radiator or blackbody.

To accomplish the thermal calibration of water only, a heirarchical classification of the TM data had to be performed, i.e., one of the middle IR (1.55 - 1.75 μm) bands was utilized to discriminate the water pixels from all the other cover types using the LARSYS layered classifier [12,16,17]. Once all the water pixels were separated from everything else, their thermal IR responses (relative digital counts) were converted to radiant temperatures. Figure 10 shows the decision tree utilized to carry out the heirarchical or layered classification and calibration of the water bodies present in the test site. Figures 11 and 12 show the images of the test site corresponding to the 1.55-1.75μm and 10.4-12.5μm bands, respectively.

The conversion of the relative thermal IR responses into radiant temperature measurements was accomplished using a non linear calibration function derived specifically for the TM thermal IR band and the range of temperatures of the two internal calibration reference blackbodies.

The non-linear calibration function was derived through the integration of Planck's equation for a spectral band covering the 10.4-12.5μm spectral range, and for a range of temperatures between 260 K and 320 K [18] at increments of 0.1 K. The resulting in-band radiances (in Watts/cm^2-sr) were then plotted versus the corresponding temperatures, as illustrated in Figure 13. Note in this figure that if one assumes a linear relationship between the emitted energy from a blackbody and its temperature for a range of temperatures in excess of 10 K (the range between the cold and hot internal calibration sources of the TM system is 60 K), errors on the order of 4 K (4°C) would be introduced.

The non-linear calibration function is given by Equation 1 below:

$$T(°C) = -12.5809 + 0.2917D - 0.00233D^2 \quad (1)$$

where: T = temperature in degrees Celsius

D = relative digital counts for the TM thermal IR band

If a linear interpolation was performed, the linear calibration function would be represented by Equation 2:

$$T(°C) = -13 + 0.23529D \quad (2)$$

The pixels of water at the intake (Kankakee River) have a relative thermal IR response equal to 95 digital counts, and those corresponding to the water at the entrance of the cooling pond equal to 135 digital counts. If these two relative thermal responses (digital counts) are substituted in Equation 1, one obtains the following radiant temperatures:

Digital Count	Radiant Temperature
95	13.1°C
135	22.6°C

Since at the time the TM data were recorded (October 25, 1982 at 16:02 GMT) reference (ground truth) data were not being collected, it was not possible to assess reliably the accuracy of the radiant temperatures derived from the TM thermal IR data. However, the personnel from the Dresden nuclear power plant keep a record of the temperature of the water at the entrance to the cooling lake. The temperature recorded for that date was 71°F or 21.7°C, which is a difference of approximately 1°C with respect to the radiant temperature derived from the TM thermal IR data. Figure 14 shows a temperature map of the Dresden power plant test site.

Although neither the temperature of the water recorded at the power plant nor the precise temperature of the internal calibration reference blackbodies in the TM system was reliable, the results obtained during this preliminary assessment of the TM radiometric data quality are very encouraging.

Summary and Conclusions

Landsat-4 thematic mapper and multispectral scanner data quality was evaluated using data from several frames over midwestern United States. Four categories of evaluation were presented:

1. Basic radiometric and geometric characteristics.

2. Overall TM system resolution.

3. Spectral dimensionality.

4. Spectral class separability.

5. Use of TM thermal IR data for temperature mapping of water bodies.

The overall quality of the TM data is very good with only a few error conditions, which in the case of band-to-band misregistration can be corrected by ground processing.

Detector-to-detector calibration was very good, such that striping should be minimal in TM. MSS demonstrated more noise problems, primarily due to high frequency wave patterns. In general, the MSS appeared somewhat noisier than previous Landsat MSS data.

The resolution estimation experiments resulted in relatively wide half-amplitude widths for the point-spread function of the TM. The reason for this is not understood; it is likely due to a combination of system and

atmospheric effects plus the uncertainty in the actual shape of the step edges being used as a test input.

Dimensionality was investigated using principal components analysis. The results indicate two significant dimensions in the MSS and up to four in the TM. The spectral analysis was the most revealing by producing twice as many separable classes in TM than in MSS. The result was due both to the greater number of spectral bands and to greater spatial resolution of the TM. More classes, such as beach, roads, field edges, and other small features, were separated out in TM where they are mixtures in MSS and in many cases not spectrally distinct. These results further verify the high quality of the TM data and promise significant increase in usefulness of these data in earth resources applications.

The radiometric quality of the TM thermal IR band was studied using both a linear calibration function and a non linear calibration function derived from the integration of Plank's equation for a spectral band covering the 10.4 - 12.5μm spectral range, and for a range of temperatures between 260 K and 320 K at increments of 0.1 K. These preliminary results support the use of the non linear calibration function with the thermal IR band for effective use of the thermal band for temperature mapping of water bodies.

Acknowledgement

Sincere appreciation is extended to Ms. Kay Hunt, systems analyst at LARS, who carried out the data formatting and data-set preparation tasks necessary before any of the analysis work could be done.

References

1. Bartolucci, L.A., M.E. Dean, P.E. Anuta, "Evaluation of the Radiometric Quality of the TM Using Clustering and Multispectral Distance Measures," Proc. Landsat-4 Scientific Characterization Early Results Symposium, NASA Goddard Space Flight Center, Greenbelt, MD, Feb. 22-24, 1983. To be published.

2. Goddard Space Flight Center, Greenbelt, MD 20771, Specifications for the Landsat-D System, Revision C, Mar. 1981, pp. 3-88.

3. McGillem, C.D., P.E. Anuta, E. Malaret, K.B. Yu, "Estimation of a Remote Sensing System Point-Spread Function From Measured Imagery,", Proc. 9th Intl. Symp. on Machine Processing of Remotely Sensed Data, LARS/Purdue University, West Lafayette, IN, June 21-23, 1983, pp. 62-68.

4. McGillem, C.D., E. Malaret, P.E. Anuta, "Resolution Estimation for the Landsat-4 Thematic Mapper,", Proc. of Conf. on Techniques for Extraction of Information from Remotely Sensed Images, Society of Photographic Scientists and Engineers, Springfield, MD. To be published.

5. Morrison, D.F. 1967. Multivariate Statistical Methods, McGraw-Hill Book Company, New York. 415pp.

6. Swain, P.H., T.V. Robertson, A.G. Wacker, "Comparison of the Divergence and B-Distance in Feature Selection", LARS/Purdue University. LARS Information Note 020871, 1971.

7. Kettig, R.L. and D.A. Landgrebe.1975. Classification of Multispectral Image Data by Extraction and Classification of Homogeneous Objects. LARS Information Note 062375, LARS/Purdue University, West Lafayette, IN, 47906-1399. 18pp.

8. Latty, R.S. 1981. Computer-Based Forest Cover Classification Using Multispectral Scanner Data of Different Spatial Resolutions. LARS Technical Report 052081, LARS/Purdue University, West Lafayette, IN 47906-1399. 186pp.

9. Bauer, M.E., P.H. Swain, R.P. Mroczynski, P.E. Anuta, and R.B. MacDonald, "Detection of Southern Corn Leaf Blight by Remote Sensing Techniques," Proceedings of the Seventh International Symposium on Remote Sensing of the Environment, Vol.1, May 17-21, 1971, pp.693-704.

10. Kumar,R. and L.F. Silva, "Emission and Reflectance from Healthy and Stressed Natural Targets with Computer Analysis of Spectroradiometric and Multispectral Scanner Data," LARS Information Note 072473, Laboratory for Applications of Remote Sensing, Purdue University, West Lafayette, Indiana, July 1973.

11. Atwell, B.H., R.B. MacDonald, and L.A. Bartolucci, "Thermal Mapping of Streams from Airborn Radiometric Scanning," Water Resources Bulletin,

Journal of the American Water Resources Association, Vol. 8, No. 2, Urbana, Illinois, April 1971.

12. Bartolucci, L.A., R.M. Hoffer, and T.R. West, "Computer-Aided Processing of Remotely-Sensed Data for Temperature Mapping of Surface Water from Aircraft Altitudes," LARS Information Note 042373, Laboratory for Applications of Remote Sensing, Purdue University, West Lafayette, Indiana, April 1973.

13. Bartolucci, L.A., R.M. Hoffer, and J.R. Gammon, "Effects of Altitude and Wavelength Band Selection on Remote Measurements of Water Temperature," Proceedings of the First PanAmerican Symposium on Remote Sensing, Panama City, Panama, May 1973.

14. Hoffer, R.M. and L.A. Bartolucci, "Remote Sensing Techniques for Measurements of Water Temperature," LARS Information Note 111671, Laboratory for Applications of Remote Sensing, Purdue University, West Lafayette, Indiana, 1971.

15. Bartolucci, L.A., "Hydrologic Features Survey," Chapter 4, LARS Information Note 121275, Laboratory for Applications of Remote Sensing, Purdue University, West Lafayette, Indiana, 1975.

16. Bartolucci, L.A., P.H. Swain, and C.L. Wu, "Selective Radiant Temperature Mapping Using a Layered Classifier," Journal of the IEEE Geoscience Electronics, Bol. GE-14, No. 2, April 1976. Also Available as LARS Information Note 111175, 1975.

17. Wu, C.L., D.A. Landgrebe, and P.H. Swain, "The Decision Tree Approach to Classification," LARS Information Note 090174, Laboratory for Applications of Remote Sensing, Purdue University, West Lafayette, Indiana, September 1974.

18. Barker, T.L., "TM Sensor Description and Status," First European Landsat-4 Workshop, ESA/EARTHNET Program, Frascati, Italy, November 1982.

19. Davis, S.M., "Polk County (Iowa) Case Study," LARS Technical Report 073183, Laboratory for Applications of Remote Sensing, Purdue University, West Lafayette, IN 47906-1399, August 1983.

LIST OF TABLES

Table 1

CHANNEL-to-CHANNEL CALIBRATION EVALUATION

Deviation of Detector Mean From Grand Mean for WEBSTER CO., IOWA "A" DATA

Scan Line Sequence

Detector / Band	1	2	3	4	5	6	7	8	9	10	11	12	13	14	15	16
1	-.08	-.4	.14	-.04	.29	.32	-.38	.44	.35	.07	-.1	-.1	.49	-.24	.2	-.29
2	.53	-.41	.35	-.47	.73	-.08	.06	.18	.2	.03	-.41	-.55	-.55	-.02	.42	.05
3	.45	-.13	.19	-.05	.1	-.77	-.14	-.2	-.23	-.11	.21	-.14	-.39	.04	.43	.76
4	.2	.4	.42	.18	1.0	.9	.64	-.1	-.77	-.94	-.65	-.59	-.38	-.22	.08	-.17
5	.12	-.15	.11	-.48	.05	-.02	.49	-.25	-.05	.04	-.23	-.44	-.44	-.44	1.29	.33
6	-.29	0.0	.32	.04	.69	.25	.24	.36	-.21	.61	.17	.02	-.39	.18	.26	-.35

Table 2.

Maximum Deviations of Mean and Variance

of any Detector for MSS Bands.

	WEBSTER CO. A Data		CHICAGO A Data	
Band	Mean	Std Dev.	Mean	Std. Dev.
1	-.28	.43	.2	.16
2	.30	-.28	.2	.25
3	.82	.29	.13	.23
4	.44	.2	.11	-.12

Table 3.

Results of TM Resolution Estimation

Using Step Differentiation.

Average of 3 Test Regions

"A" Tape Data 30M Pixel Spacing

	TRIGONOMETRIC SMOOTHING				SPLINE SMOOTHING		
	W (Pix.)	Corr.	W (M)	Knots	W (Pix.)	Corr.	W (M)
Band 4	1.60	1.44	43.2	7	1.13	1.31	39.3
Band 5	1.62	1.46	43.8	7	1.29	1.49	44.7

Table 4.

Linear Regression Results of the Forward and Reverse Scans

Iowa TM "A" Tape (Scene ID:40049-16264).

Channel	Scan	R^2	Slope	Total drop in digital count across-scan
1	Forward	0.413	-0.00087	5.22
	Reverse	0.261	-0.00067	4.02
2	Forward	0.153	-0.0003	1.8
	Reverse	0.041	-0.00022	1.32
3	Forward	0.041	-0.00022	1.32
	Reverse		--------*	
4	Forward	0.06	-0.00136	8.16
	Reverse	0.148	-0.00217	13.02
5	Forward	0.127	-0.00127	7.62
	Reverse	0.275	-0.00172	10.32
7	Forward	0.058	-0.00044	2.64
	Reverse	0.077	-0.00046	

*No significant regression could be found.

Table 5.

Table of Eigenvectors (Principal Components) and Eigenvalues of the MSS "P" Tape Data for Chicago O'Hare Test Site Test Site (Scene ID: 40101-10625).

Matrix of Eigenvectors

Wavelength Band	Principal Component (Eigenvector) 1	2	3	4
1	0.39291	-0.41975	0.36717	0.73117
2	0.51763	-0.57144	-0.54223	-0.33392
3	0.64029	0.31652	0.54675	-0.43693
4	0.40951	0.63015	-0.52176	0.40371

Eigenvector	Eigenvalue	Percent Variance	Cumulative Percentage
1	68.83	65.30%	65.30%
2	33.18	31.48%	96.78%
3	1.98	1.88%	98.66%
4	1.42	1.34%	100.00%

Table 6.

Table of Eigenvectors (Principal Components) and Eigenvalues of the TM "P" Tape Data for the Chicago O'Hare Test Site (Scene ID: 40101-10625).

	Principal Component (Eigenvector)						
Waveband	1	2	3	4	5	6	7
1	0.389	-0.484	0.335	-0.104	-0.213	-0.666	-0.057
2	0.258	-0.244	-0.189	-0.009	-0.024	0.361	0.841
3	0.376	-0.357	0.173	-0.065	-0.051	0.639	-0.535
4	0.231	0.599	0.728	0.070	0.224	-0.013	-0.048
5	0.639	0.456	-0.436	-0.157	-0.410	-0.025	0.032
7	0.421	-0.103	-0.321	0.254	0.792	-0.133	-0.005
6	0.047	-0.021	0.010	0.944	-0.325	0.007	-0.025

Eigenvector	Eigenvalue	Pct of Var	Cum Pct
1	402.90	71.84%	71.84%
2	102.29	18.24	90.07
3	41.37	7.38	97.45
4	5.90	1.05	98.50
5	4.96	0.88	99.39
6	2.20	0.39	99.78
7	1.24	0.22	100.00

Table 7.

Spectrally Separable Classes in TM and MSS Data of Des Moines, Iowa Area.

CLASS NUMBER	TM CLASS NAME	EXISTS in MSS	CLASS NAME	TM CLASS NAME	EXISTS in MSS
1	Forest1	x	22	Substation	
2	Forest2	x	23	Quarry	
3	Corn1	x	24	Concrete	x
4	Corn2		25	Sludge	x
5	Soy1	x	26	Industrial1	
6	Soy2	x	27	Industrial2	
7	Soy3	x	28	Urban/Hiway	x
8	Soy4	x	29	Soil/Hiway	
9	Soy5	x	30	Residential1	x
10	Soy6	x	31	Residential2	x
11	Wheat Residue	x	32	Beach1	
12	Grass1	x	33	Beach2	
13	Grass2		34	Beach3	
14	Grass3		35	Soilwet1	
15	Soil/Veg1		36	Soilwet2	
16	Soil/Veg2		37	Marsh	
17	Soil/Veg3		38	Water1	x
18	Farm/Grass		39	Water2	x
19	Road/Farm		40	Water3	x
20	Baresoil1	x	41	Water4	x
21	Baresoil2		42	Water5	

Table 8.

Separability (Transformed Divergence)

for 42 Classes in Thematic Mapper Data.

CHANNEL COMBINATIONS	DIVERGENCE MIN.	AVE.	BEST CHANNELS
1	1	1574	5
2	210	1880	4 5
3	522	1949	3 4 5
4	1090	1973	3 4 5 6
5	1356	1979	3 4 5 6 7
6	1405	1983	2 3 4 5 6 7
7	1553	1986	1 2 3 4 5 6 7

Table 9.

Separability for 21 Classes in MSS Data.

CHANNEL COMBINATIONS	DIVERGENCE MINIMUM	AVERAGE
3	32	1842
2 3	730	1957
2 3 4	1032	1968
1 2 3 4	1112	1973

Table 10.

Classification Accuracy and CPU Time Comparison

on Test Data in the Des Moines Area.

Scene ID: 40049-16264

CLASS	TM GML Per-Point Classifier (All 7 Bands) %Correct	TM GML Per-Point Classifier (Best 4 Bands) %Correct	TM SECHO Classifier (All 7 Bands) %Correct	MSS GML Per-Point Classifier (All 4 Bands) %Correct
Forest	99.0	97.1	100.0	91.2
Corn	92.0	76.8	97.7	30.8
Soybeans	100.0	99.8	100.0	99.3
Bare Soil	99.7	99.0	100.0	55.6
Grass	96.8	87.6	98.1	1.9
Water	100.0	96.8	100.0	98.9
Urban	91.7	99.9	95.8	50.2
Overall	95.7	92.6	97.9	67.4

	No. of Classes	No. of pixels Classified	No. of bands	CPU Time (hours)
MSS	21	250,000	4	0.4
TM	42	1,000,000	4	2.7
TM	42	1,000,000	7	7.9

LIST OF FIGURES

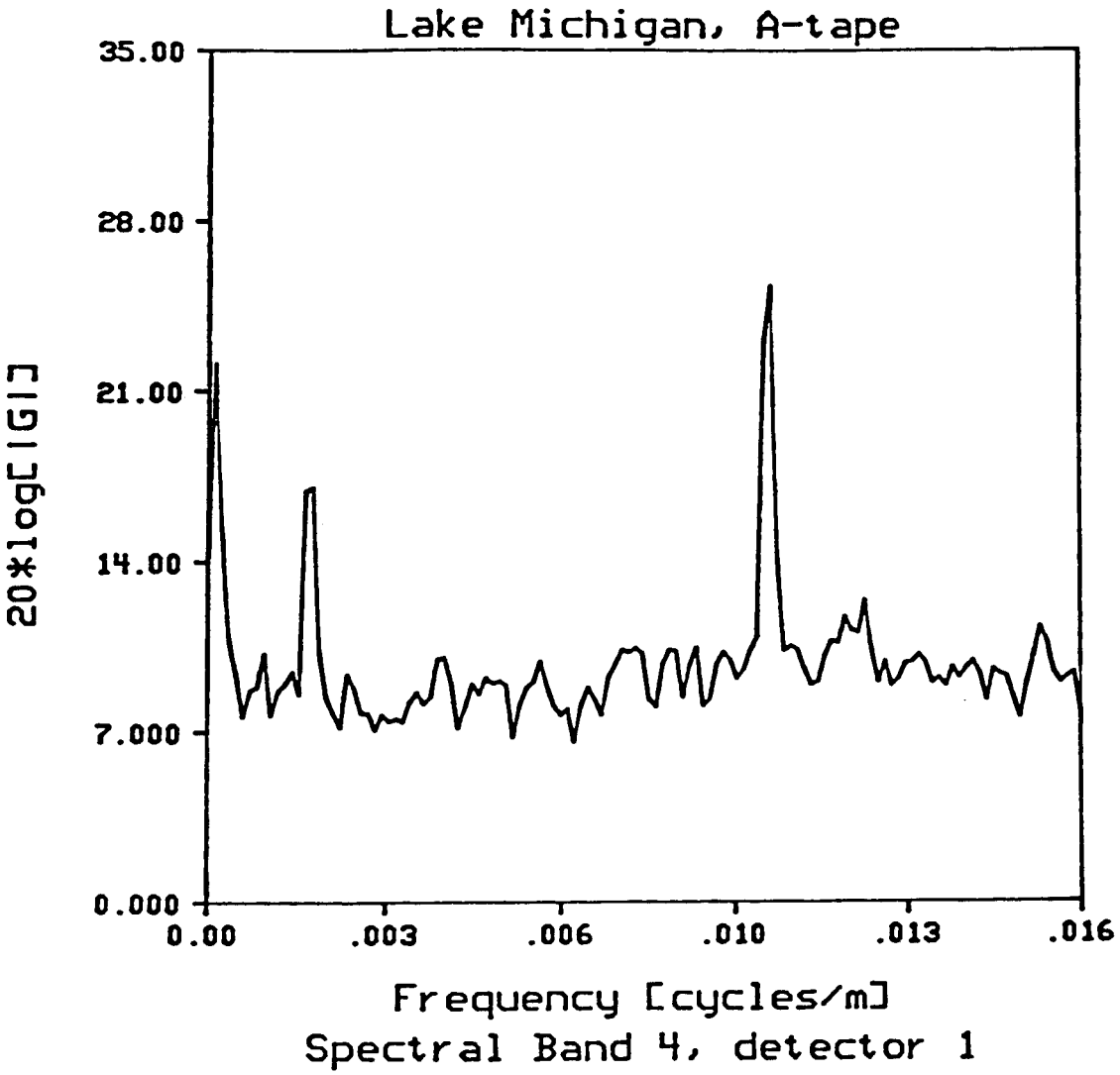

Figure 1. Power Spectrum of Low Level TM Data Showing Noise Peaks at Two Frequencies: 3.12 pixels and 17 pixels per cycle.

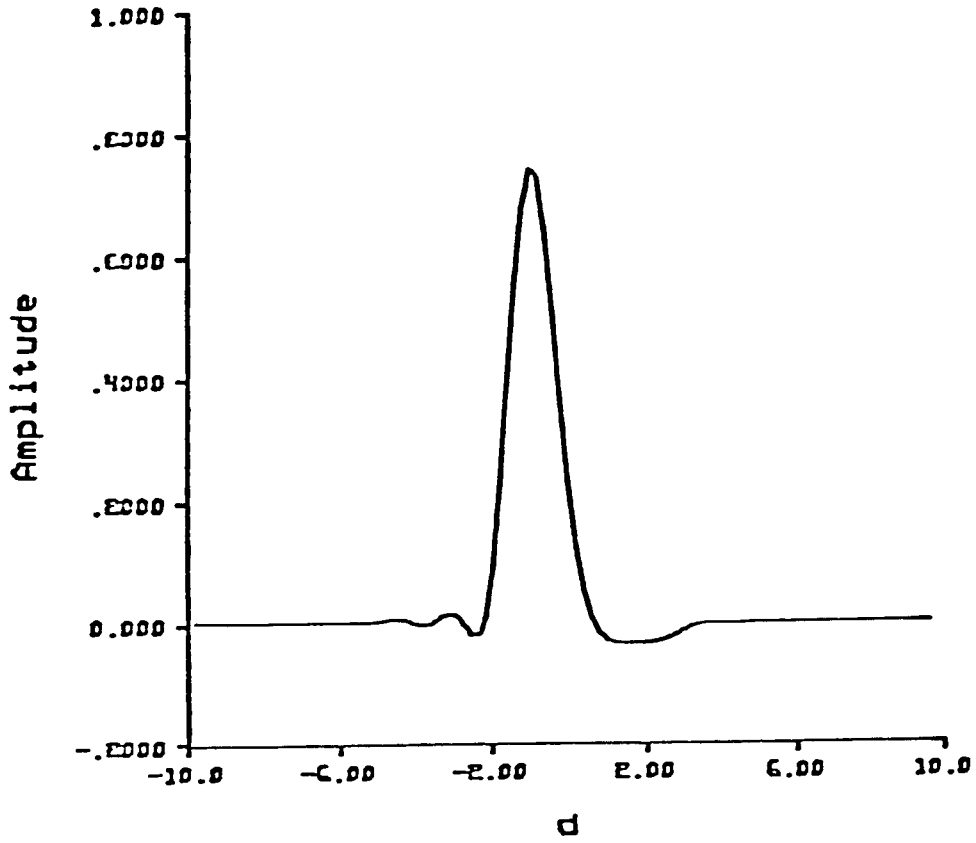

Figure 2. TM Band 4 Point Spread Function Estimate Using Trigonometric Smoothing with 29 Coefficients.

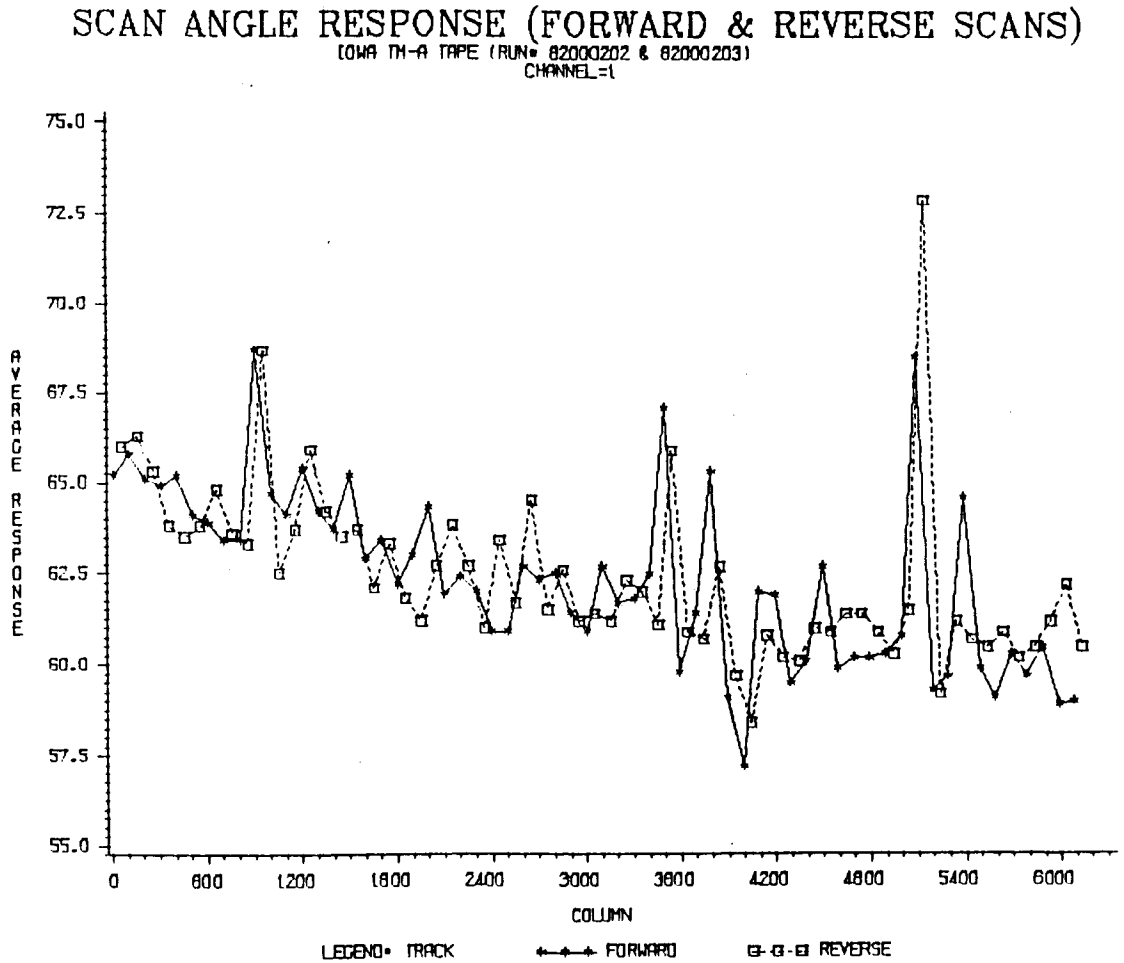

Figure 3. Mean Scan Angle Response for Band 1 Showing 5 Digital Count Variation Over Width of Frame.

MSS Band 1 (0.5 - 0.6μm)

MSS Band 2 (0.6 - 0.7μm)

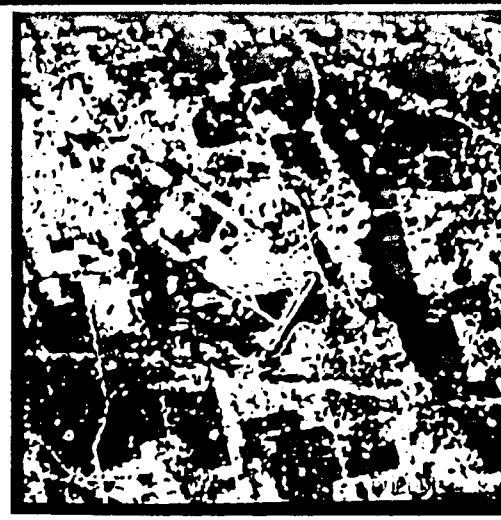

MSS Band 3 (0.7 - 0.8μm)

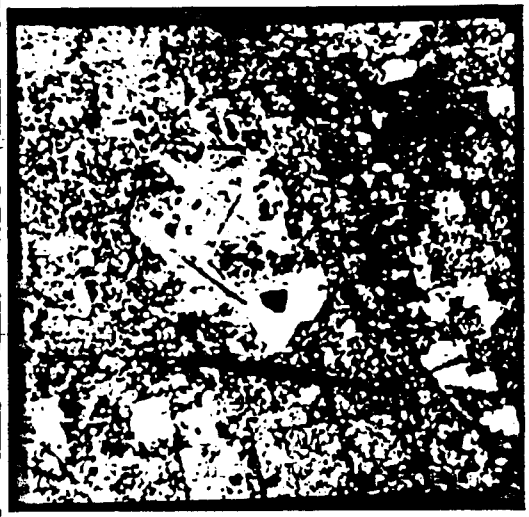

MSS Band 4 (0.8 - 1.1μm)

MSS PC1

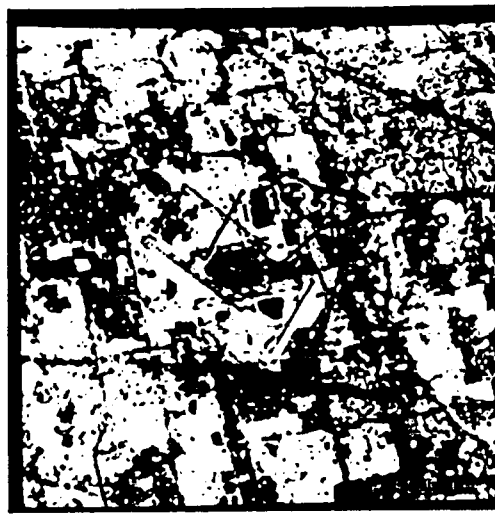

MSS PC2

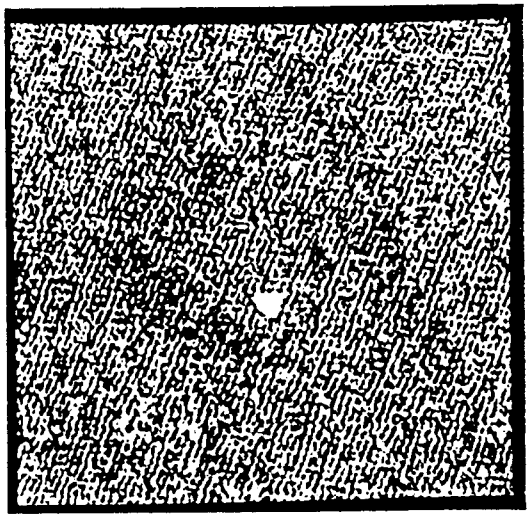

MSS PC3

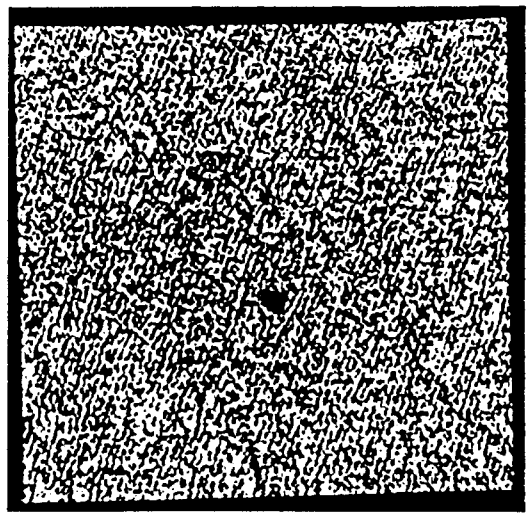

MSS PC4

Figure 4. Images of Bands 1-4 and Principal Components 1-4 of Landsat IV MSS of the Chicago O'Hare Test Site.

TM PC1

TM PC2

TM PC3

TM PC4

TM PC5

TM PC6

TM PC7

Figure 5. (Continued)

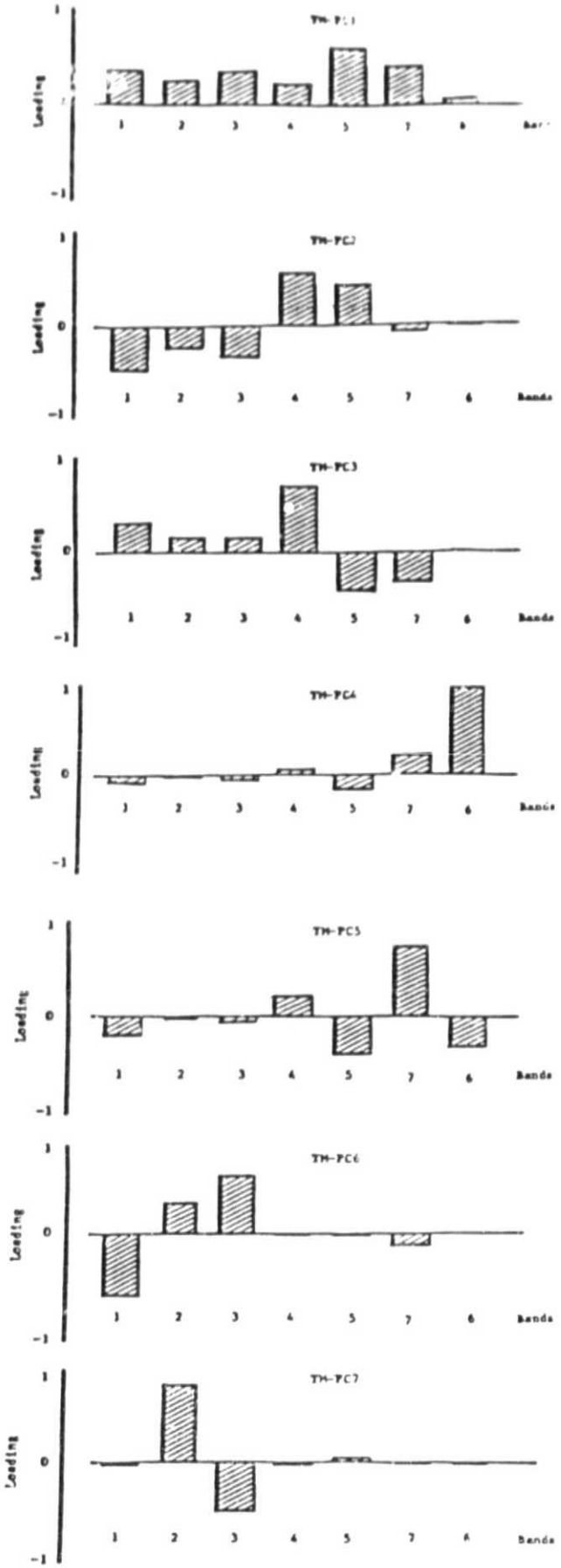

Figure 6. The Loadings or Coefficients of the Original Wavelength Bands on Each of the Ordered TM Principal Components of the Chicago O'Hare Test Site.

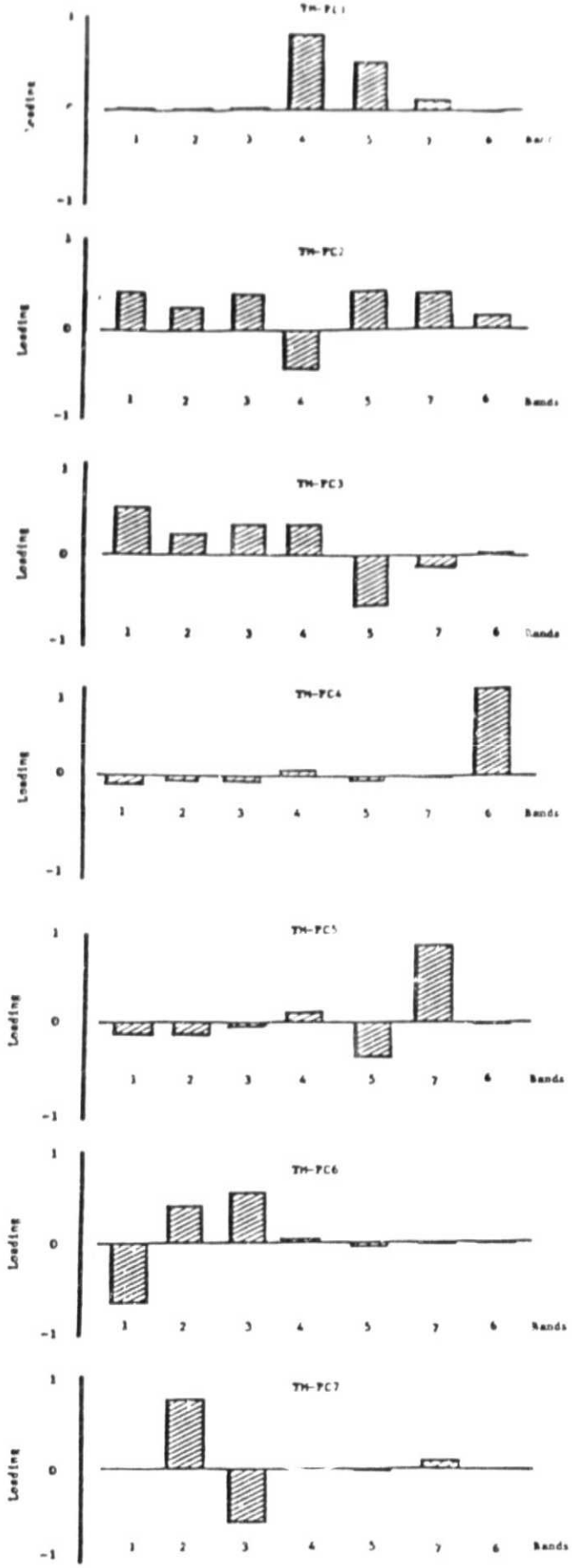

Figure 7. The Loadings or Coefficients of the Original Wavelength Bands on Each of the Ordered TM Principal Components of the Des Moines Iowa Test Site.

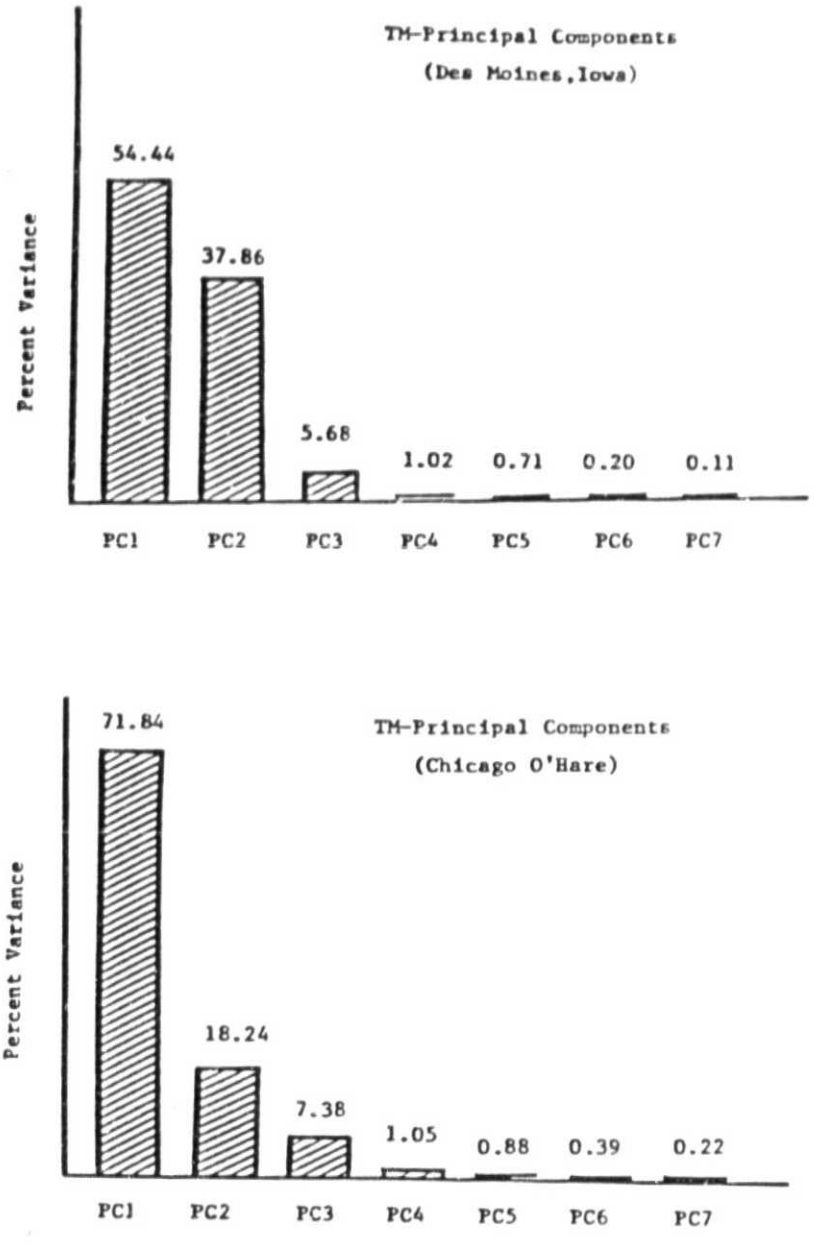

Figure 8. Percent of Total Variance Accounted for by Each of the Ordered TM Principal Components of the Des Moines Iowa and Chicago O'Hare Test Data Sets.

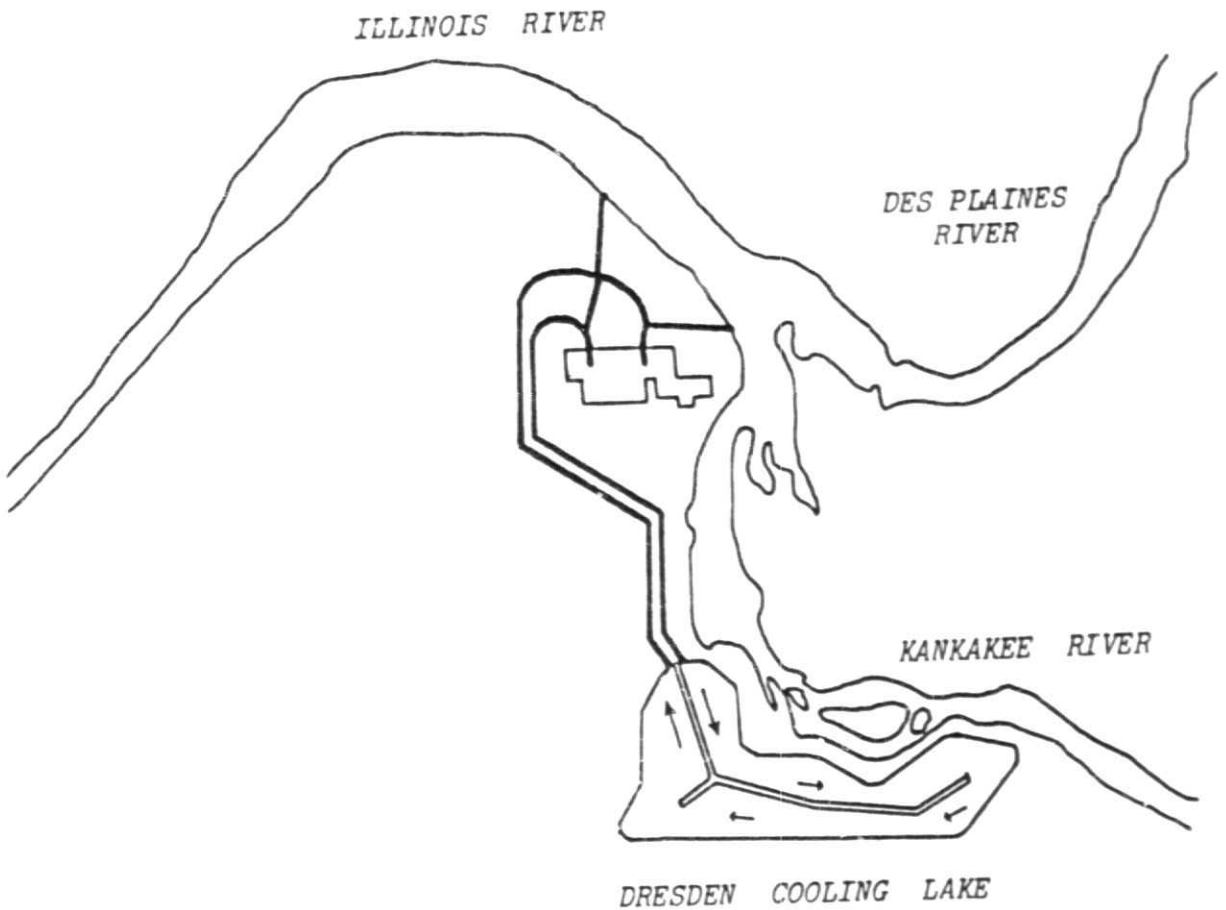

Figure 9. Schematic Diagram of the Dresden Nuclear Power Plant, Channels, Cooling Lake and the Kankakee, Des Plaines and Illinois Rivers.

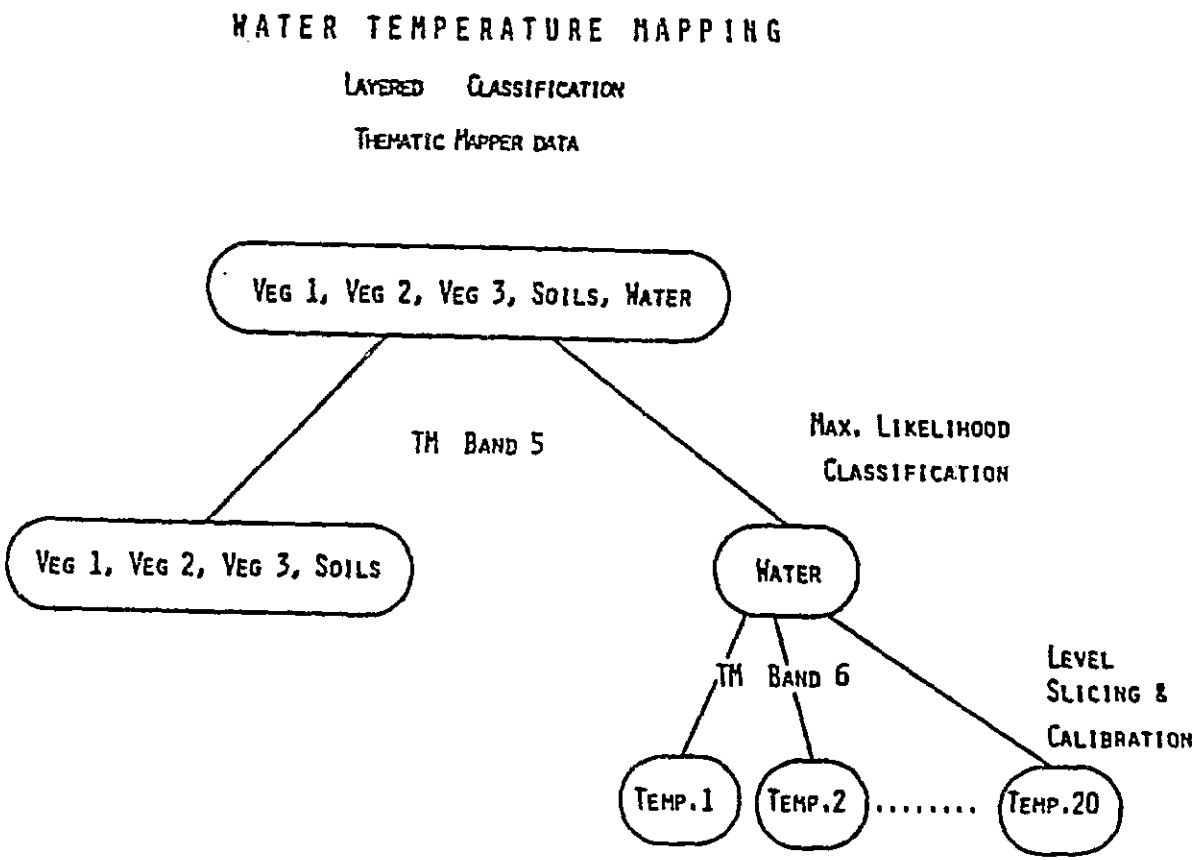

Figure 10. Decision Tree Utilized to Carry out the Hierarchical Classification and Calibration of the Water Bodies Present in the Dresden Nuclear Power Plant Test Site.

Figure 11. Image of Band 5 (1.55 - 1.75μm) of Landsat IV TM of the Dresden Power Plant Test Site.

Figure 12. Image of Band 6 (10.4 - 12.5μm) of Landsat IV TM of the Dresden Power Plant Test Site.

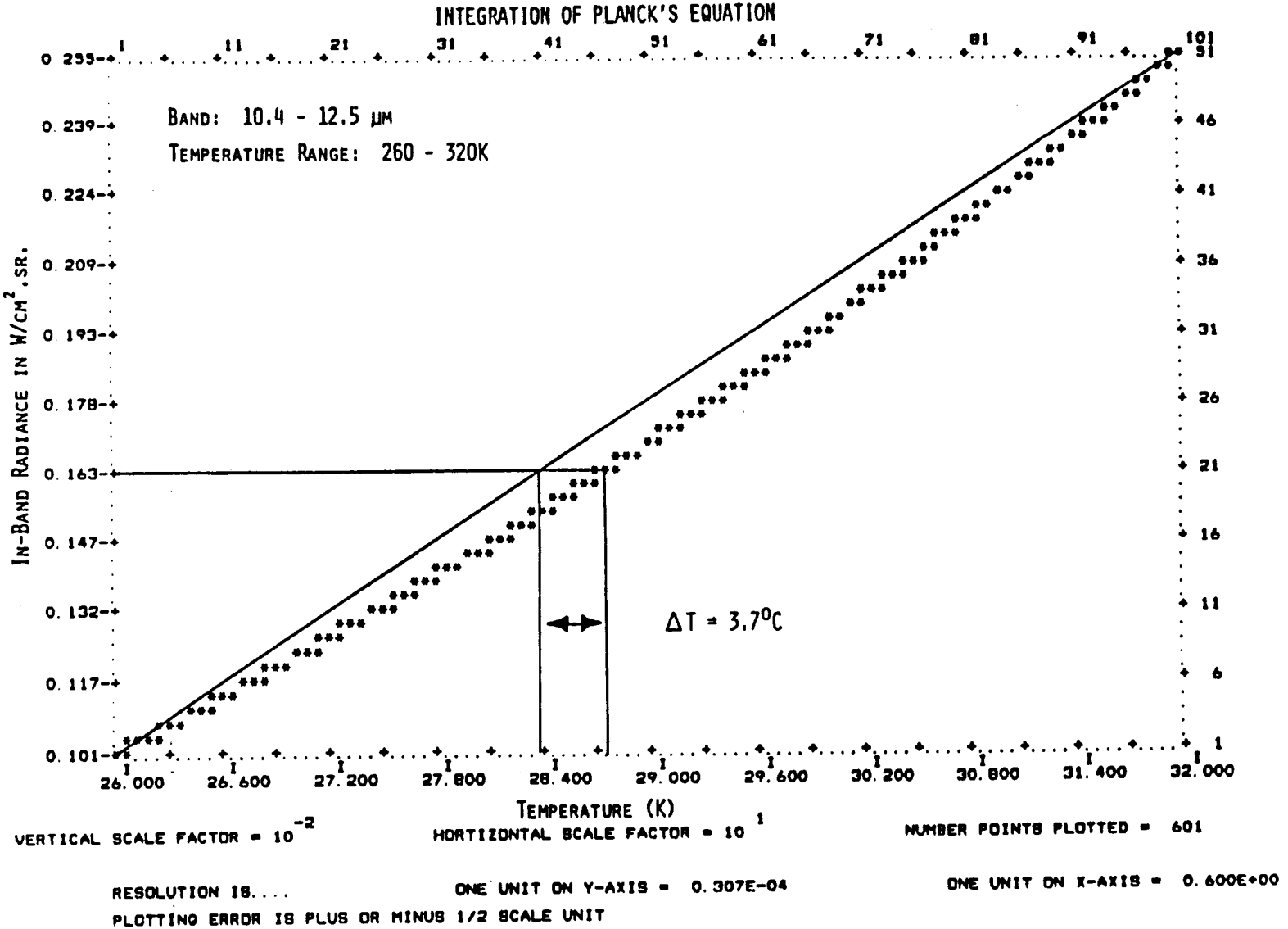

Figure 13. Integration of Planck's Equation for a Spectral Band Covering the 10.4 - 12.5µm Spectral Range, and for a Range of Temperatures Between 260 K and 320 K at 0.1 K increments.

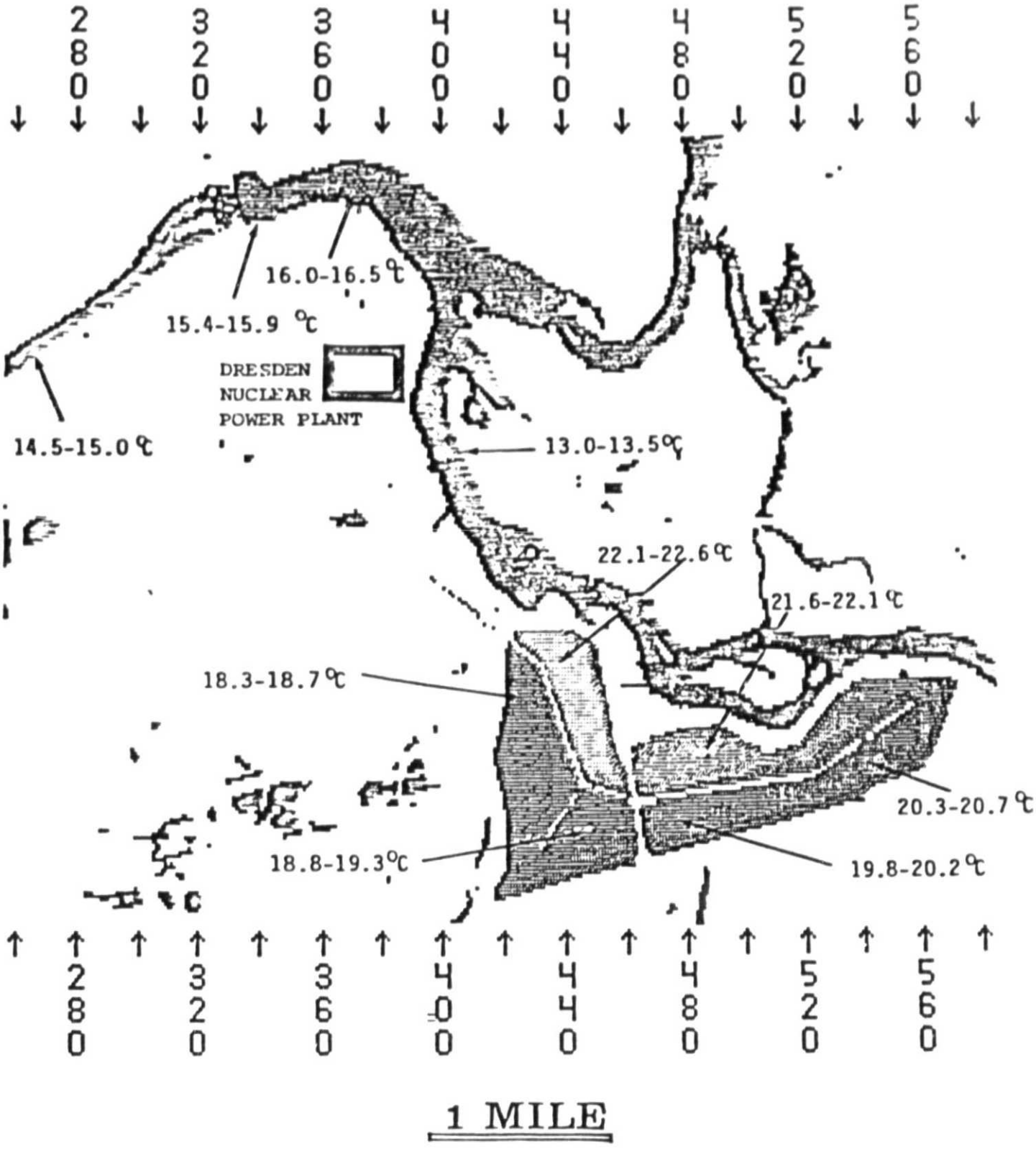

Figure 14. Temperature Map of the Dresden Nuclear Power Plant Test Site Derived from the Landsat-IV TM Data.